Investigations of three-, four-, and five-particle decay channels of levels in light nuclei created using a ^{9}C beam

R. J. Charity, J. M. Elson, J. Manfredi, R. Shane, and L. G. Sobotka

Departments of Chemistry and Physics, Washington University, St. Louis, Missouri 63130, USA

B. A. Brown, Z. Chajecki, D. Coupland, H. Iwasaki, M. Kilburn, Jenny Lee, W. G. Lynch, A. Sanetullaev, M. B. Tsang, J. Winkelbauer, and M. Youngs

National Superconducting Cyclotron Laboratory and Department of Physics and Astronomy, Michigan State University, East Lansing, Michigan 48824, USA

S. T. Marley, D. V. Shetty, and A. H. Wuosmaa

Department of Physics, Western Michigan University, Kalamazoo, Michigan 49008, USA

T. K. Ghosh

Variable Energy Cyclotron Centre, 1/AF Bidhannagar, Kolkata 700064, India

M. E. Howard

Department of Physics and Astronomy, Rutgers University, New Brunswick, New Jersey 08903, USA

The interactions of an $E/A = 70$-MeV ^{9}C beam with a Be target was used to populate levels in Be, B, and C isotopes, which undergo decay into many-particle exit channels. The decay products were detected in the HiRA array and the level energies were identified from their invariant mass. Correlations between the decay products were examined to deduce the nature of the decays, specifically to what extent all the fragments were created in one prompt step or whether the disintegration proceeded in a sequential fashion through long-lived intermediate states. In the latter case, information on the spin of the level was also obtained. Of particular interest is the five-body decay of the ^{8}C ground state, which was found to disintegrate in two steps of two-proton decay passing through the ^{6}Be$_{g.s.}$ intermediate state. The isobaric analog of ^{8}C$_{g.s.}$ in ^{8}B was also found to undergo two-proton decay to the isobaric analog of ^{6}Be$_{g.s.}$ in ^{6}Li. A 9.69-MeV state in ^{10}C was found to undergo prompt four-body decay to the $2p + 2\alpha$ exit channel. The two protons were found to have a strong enhancement in the diproton region and the relative energies of all four p-α pairs were consistent with the ^{5}Li$_{g.s.}$ resonance.

PACS number(s): 21.10.−k, 25.70.Ef, 25.60.−t, 27.20.+n

I. INTRODUCTION

The ground and excited states of many light proton-rich nuclei decay by the emission of protons and other charged particles. A number of these states disintegrate into just protons and α particles and other very light fragments. Well-known examples are the ground states of ^{6}Be and ^{9}B, which decay to the $2p + \alpha$ and the $p + 2\alpha$ exit channels. Such states can be studied with resonance decay spectroscopy where all of the decay fragments are detected. The excitation energy of the parent state can be determined from the invariant mass of the detected decay products. For exit channels with more than two fragments, the angular and energy correlations between the fragments can provide information on the spin of the state and the nature of its decay, i.e., whether the decay proceeds through a series of sequential two-body decay steps or via a more prompt process.

In this work we have utilized a ^{9}C beam to study a number of such states which were formed via nucleon knockout and more complicated reactions. Of particular interest is the ground state of ^{8}C, which is known to be unstable to the five-body exit channel $4p + \alpha$. Information about ^{8}C is rather sparse and the five-body exit channel has never been observed

experimentally. A particular question for ^{8}C disintegration and other many-particle exit channels detected in this work is whether the final particles were created in one fast process or in a series of sequential steps with the creation of long-lived intermediate states. Of course there is not always a clear demarcation between such processes. If the lifetime of the intermediate states becomes too short, does it make sense to still describe the decay as two or more sequential steps?

One situation that is particularly clear is the two-proton decay described by Goldansky [1] where no intermediate state can be energetically accessed. Examples of this are the two-proton decays of ^{45}Fe [2] and ^{54}Zn [3]. In cases where this condition is not reached, Bochkarev *et al.* [4] considered a distinction in the decay type based on the width of the potential intermediate state. For a three-body exit channel, if the potential intermediate state has a width Γ_I, which is of the same magnitude as the kinetic energy E_k^1 released in the decay to this state, then its decay was deemed democratic, i.e., all energy scales in the subsystems and the three-body systems are comparable. We have constructed the ratio

$$R_E = \frac{\Gamma_I}{E_k^1} \tag{1}$$

to quantify this. Thus if $R_E \ll 1$, the decay is sequential, whereas if $R_E \gtrsim 1$, then the decay is democratic. Large values of Γ_I and thus of R_E imply a short-lived intermediate state and thus a difficulty in distinguishing the two decay steps. Another way to quantify this is to estimate the separation d_E of the fragments from the first step at the average time of the second decay step, i.e., the decay of the the intermediate state. This separation is

$$d_E = \sqrt{\frac{2E_k^1}{\mu}} \frac{\hbar}{\Gamma_I}, \qquad (2)$$

where μ is the reduced mass of products produced in the first decay step. If d_E is much larger than the typical nuclear diameter ($\sim$5 fm), then the two decay steps are well separated and cannot influence each other through nuclear processes.

Again we emphasize that the quantities R_E and d_E do not provide sharp distinctions between prompt and sequential processes. For intermediate values of these quantities, one may consider a decay process that is basically sequential, but where final-state interactions between the products from the different decay steps are still important. If these final-state interactions do not wash out sequential signals, such as the invariant mass of the intermediate state deduced from its decay products, or the angular correlations between the sequential decay steps, then one might still claim that the decay has a strong sequential character. However, detailed predictions for the correlations may require a many-body calculation.

The angular correlations in sequential decay are a consequence that the system passes through an intermediate state of well defined spin. Not all potential sequential decay scenarios have such correlations, for example if the intermediate state is $J = 0$, or the orbital angular momentum removed in either step is zero. Thus the search for these correlations cannot be performed for all cases.

An example of a truly sequential process is the decay of the ground state of ^{9}B to the $p + 2\alpha$ exit channel. The decay begins by a proton emission to the ground state of ^{8}Be, which has a very small width ($\Gamma_I = 6.8$ eV). Here, $R_E = 3.6 \times 10^{-5}$ and $d_E = 6.1 \times 10^5$ fm, which indicates that there are no significant interactions between the proton from the first step and the α particles from the second step.

The nucleus ^{6}Be$_{g.s.}$ which decays to the $2p+\alpha$ channel provides an example of democratic decay. The possible intermediate state ^{5}Li$_{g.s.}$ is very wide ($\Gamma_E = 1.23$ MeV), but most of the strength associated with this state is energetically inaccessible in ^{6}Be$_{g.s.}$ decay (see Fig. 3). Sequential decay is only possible through the low-energy tail of this resonance. Thus ^{6}Be$_{g.s.}$ is almost a Goldansky-type decay. In a sequential scenario, the mean energy released in the first step can be determined in an R-matrix approximation (Sec. III) as $E_k^1 = 0.64$ MeV and this gives $R_E = 1.92$ and $d_E = 6.5$ fm, which is not in the realm of a truly sequential decay. Experimental studies show no evidence of the angular correlations expected in a sequential scenario [5] (see also Sec. IV A) and a good description of the decay correlations, the decay energy, and its width can be obtained with a three-body cluster model [6].

In this work we report on an experimental investigation of particle-unstable states in Be, B, and C isotopes, all of which

undergo disintegration into three or more final fragments. In each case, we have measured correlations between these fragments to deduce the nature of the decay and to determine to what extent sequential and prompt many-body processes are involved. The states reported on were all created as projectilelike fragments after the interaction of a secondary $E/A = 70$ MeV ^{9}C beam with a Be target. One case of particular interest is the $4p + \alpha$ decay of ^{8}C$_{g.s.}$. As ^{6}Be$_{g.s.}$ is a possible intermediate state in the decay of this level, we have obtained improved data for the ^{6}Be system using a $E/A = 70$ MeV ^{7}Be secondary beam to help in the interpretation of the ^{8}C data. Some of the ^{8}C results have already been published in Ref. [7]. The details of the experiment are discussed in Sec. II. Results for each of the examined states are given in Sec. IV and the conclusions of this work are presented in Sec. V.

II. EXPERIMENTAL METHOD

A primary beam of $E/A = 150$-MeV ^{16}O was extracted from the Coupled Cyclotron Facility at the National Superconducting Cyclotron Laboratory at Michigan State University with an intensity of 125 pnA. This beam bombarded a ^{9}Be target producing $E/A = 70.0$-MeV ^{9}C and ^{7}Be projectile-fragmentation products which were selected by the A1900 separator with a momentum acceptance of $\pm$0.5%. The ^{9}C secondary beam had an intensity of 1.6×10^5 s^{-1} with a purity of $\sim$65% with the main contaminant being ^{6}Li. The ^{7}Be beam had an intensity of 4×10^7 s^{-1} with a purity of $\sim$90%.

The two secondary beams impinged on a 1-mm-thick target of ^{9}Be. Charged particles produced in the reactions with this target were detected in the HiRA array [8]. For this experiment, the array consisted of 14 E-ΔE [Si-CsI(Tl)] telescopes located at a distance 90 cm downstream from the target. The angular coverage of the array is illustrated in Fig. 1 and it subtended polar angles from 1.4° to 13°. Each telescope consisted of a 1.5-mm-thick, double-sided Si strip ΔE detector followed by a 4-cm-thick CsI(Tl) E detector. The ΔE detectors are 6.4 cm × 6.4 cm in area with each of the faces divided into 32 strips. Each E detector consisted of four separate CsI (Tl) elements each spanning a quadrant of the preceding Si detector. Signals produced in the 896 Si strips were processed with the HINP16C chip electronics [9]. For the ^{9}C beam, the time of flight measured between a thin scintillator foil in the A1900 extended focal plane and the HiRA trigger was used in conjunction with the energy loss in this foil to reject most of the beam contaminants.

The energy calibration of the Si detectors was obtained with a ^{228}Th α-particle source. The particle-dependent energy calibrations of the CsI detectors were achieved with cocktail beams selected with the A1900 separator. These include protons ($E/A = 60$ and 80 MeV), α particles ($E/A = 60$ and 80 MeV), deuterons ($E/A = 21$ and 59 MeV), tritons ($E/A = 27$ and 36 MeV), ^{3}He ($E/A = 37$ and 103 MeV), and ^{6}Li ($E/A = 60$ and 80 MeV) beams.

The HiRA telescopes have excellent isotope separation for the all of the light fragments of interest in this work and multiple fragments within a single telescope can be identified [10]. The gains for the Si amplifiers were set up for the
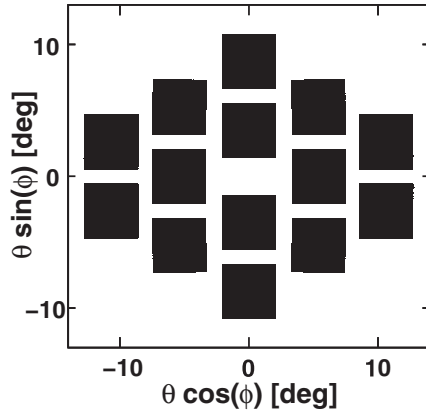
FIG. 1. The angular coverage of the HiRA array used in this experiment.

detection of hydrogen and helium isotopes. Some information on lithium isotopes is used in this work, but lower-energy Li fragments saturated the Si shaping amplifiers and could not be identified (see later).

III. SIMULATIONS

The effect of the detector acceptance and resolution is quite important when extracting decay widths, branching ratios, and correlations between the fragments. These effects have been extensively studied using Monte Carlo simulations that include the angular acceptance and the angular and energy resolutions of the detectors, the energy loss [11] and small-angle scattering [12] of the fragments as they leave the target, and the beam-spot size. These simulations have proven quite reliable in past experiments with HiRA [10,13].

A number of different types of simulations are described in this work including both sequential and prompt decay processes. However, the predicted resolution of the excitation energy of a level was found to be mostly insensitive to the details of the decay process, but is largely determined from the detector properties.

In simulating sequential three-body decays, where the width of the intermediate state is significant, we have used the R-matrix formalism [14,15] to predict the distribution of E_T, the total kinetic energy released, and $E_x = E_T - E_k^1$, the kinetic energy released in the second step;

$$N(E_T, E_x) \sim \frac{\Gamma_1(E_T, E_x)}{[E_T - Q_1 - \Delta_{\text{tot}}(E_T)]^2 + (1/4)\Gamma_{\text{tot}}^2(E_T)},$$
(3)

where

$$\Gamma_{\text{tot}}(E_T) = \int_0^{E_T} \Gamma_1(E_T, E_x) dE_x,$$
(4)

$$\Delta_{\text{tot}}(E_T) = \int_0^{\infty} \Delta_1(E_T, E_x) dE_x,$$
(5)

$$\Gamma_1(E_T, E_x) = 2\gamma_1^2 P_{1\ell}(E_T - E_x)\rho(E_x),$$
(6)

$$\Delta_1(E_T, E_x) = -\gamma_1^2 [S_{1\ell}(E_T - E_x) - S_{1\ell}(Q_1 - E_x)]\rho(E_x),$$
(7)

$$\rho(E_x) = c \frac{\Gamma_2(E_x)}{[E_x - Q_2 - \Delta_2(E_x)]^2 + (1/4)\Gamma_2^2(E_x)},$$
(8)

$$\int_0^{\infty} \rho(E_x) dE_x = 1,$$
(9)

$$\Gamma_2(E_x) = 2\gamma_2^2 P_{2\ell}(E_x),$$
(10)

$$\Delta_2(E_x) = -\gamma_2^2 [S_{2\ell}(E_x) - S_{2\ell}(Q_2)],$$
(11)

$$P_\ell(E) = \frac{ka}{F_\ell(ka)^2 + G_\ell(ka)^2},$$
(12)

$$S_\ell(E) = \frac{F'_\ell(ka)F_\ell(ka) + G'_\ell(ka)G_\ell(ka)}{F_\ell(ka)^2 + G_\ell(ka)^2},$$
(13)

$$a = 1.45 \text{ fm} (A_1^{1/3} + A_2^{1/3}).$$
(14)

F and G are regular and irregular Coulomb wave functions, k is the wave number, c is a normalization constant determined from Eq. (9), γ_1^2 and γ_2^2 are the reduced widths associated with the first and second decay steps, and Q_1 and Q_2 are the centroids associated with E_T and E_x, respectively. Angular correlations in sequential decay are calculated from Refs. [16,17].

The reduced width can be expressed as

$$\gamma^2 = S\theta_{sp}^2 \frac{\hbar^2}{\mu a^2},$$
(15)

where S is the spectroscopic factor and θ_{sp}^2, the single-particle dimensionless reduced width, is

$$\theta_{sp}^2 = \frac{a}{2} \frac{u^2(a)}{\int_0^a u^2(r) dr}.$$
(16)

Here $u(r)/r$ is the single-particle radial wave function calculated with a Coulomb plus Wood-Saxon potential with standard parameters for radii and diffuseness ($r_0 = 1.25$ fm, $r_C = 1.3$ fm, and $a = 0.65$ fm) and the depth is adjusted to fit the resonance energy.

IV. RESULTS

The deduced properties of the levels investigated in this study are summarized in Table I including their centroids, widths, and decay modes. More detailed discussions for each case are contained in the rest of this section, including comparison with the evaluated quantities from the ENSDF database [18]. Excitation energies are determined from the invariant mass method, i.e., the total kinetic energy of the fragments in their center-of-mass reference frame minus the decay Q value.

A. ^{8}C ground state

The ground state of ^{8}C is unstable to disintegration into four protons and an α particle. The distribution of ^{8}C excitation energy reconstructed from the $4p + \alpha$ channel following neutron knockout of ^{9}C beam particles is displayed in Fig. 2(a). The excitation energy was determined assuming the ^{8}C mass excess of 35.094 MeV obtained from the 2003 mass evaluation of Ref. [19]. The mass excess is needed to calculate the decay Q value. The excitation-energy spectrum shows a strong peak

TABLE I. The excitation energy, width, spin, and isospin of states for which new information is determined.

Nucleus	Decay	Branching ratio	Exit channel	E^* (MeV)	Γ (keV)	J^π	T
^{7}B	$p + {}^6$Be$_{g.s.}$	$81 \pm 10\%$	$3p + \alpha$	0.0	801 ± 20		3/2
^{8}B	$p + {}^7$Be$_{4.57}$		$p + {}^3$He $+ \alpha$	5.93 ± 0.02	850 ± 260	3, 4	1
^{8}B	$p + {}^7$Be$_{6.73}$		$p + {}^3$He $+ \alpha$	8.15 ± 0.20	950 ± 320		1
^{8}B	$2p + {}^6$Li$_{IAS}$	$\sim 97.5\%$	$2p + {}^6$Li	10.619 ± 0.009^b	$<60^b$	0^+	2
	$2p + {}^6$Li$_{2.18}$	$\sim 1.0\%$	$2p + d + \alpha$				
	$2p + d + \alpha$	$\sim 1.5\%$					
^{8}Be	$p + {}^7$Li$_{4.63}$		$p + t + \alpha$	$22.96 \pm .02$	680 ± 146	3, 4	1
^{8}C	$2p + {}^6$Be$_{g.s.}$	100%	$4p + \alpha$	0.0	130 ± 50	0^+	2
^{9}B	$\alpha + {}^5$Li	$97.2 \pm 0.5\%$	$p + 2\alpha$	11.70 ± 0.02	880 ± 80	$3/2^-, 5/2^+, 7/2^-$	1/2
	$p + {}^8$Be$_{3.03}$	$2.8 \pm 0.5\%$	$p + 2\alpha$				
^{9}B	$p + {}^8$Be$_{T=0+1}$		$p + 2\alpha$	16.99 ± 0.03	22 ± 5^b	$1/2^-$	3/2
^{9}B	$p + {}^8$Be$_{19.069}$		$2p + {}^7$Li	20.64 ± 0.10^a	450 ± 250		
^{10}C	$p + {}^9$B$_{2.345}$		$2p + 2\alpha$	8.54 ± 0.02	<200		
^{10}C	$2p + 2\alpha$	48%	$2p + 2\alpha$	9.69	490		1
	$\alpha + {}^6$Be	35%	$2p + 2\alpha$				
	$p + {}^9$B$_{2.34}$	17%	$2p + 2\alpha$				
^{10}C			$2p + 2\alpha$	10.48 ± 0.2	<200		
^{10}C			$2p + 2\alpha$	11.44 ± 0.2	<200		

^{a}Assumed decay is to the ground state of ^{7}Li.

^{b}Value from tabulations.

located near zero excitation energy indicating that we have populated the ground state of ^{8}C. The long-dashed curve shows the simulated shape, including detector response, based on the evaluated mass excess and the listed ^{8}C decay width of 230 keV. This curve also contains a background contribution, which is indicated by the short-dashed curve. The simulated shape is both wider and shifted up in energy compared to the experimental peak, suggesting that the evaluated mass excess and width used in the simulations are incorrect.

In order gain a better understanding of the magnitude of the experimental uncertainties associated with this measurement, we have investigated the line shape of the ^{6}Be ground state formed in neutron knockout reactions from the ^{7}Be beam. In the ^{9}C and ^{7}Be neutron knockout reactions, the beam velocities, target thickness, and detector apparatus were identical and thus systematic errors are expected to be the same. The reconstructed ^{6}Be excitation-energy spectrum from the detected $2p + \alpha$ events is displayed in Fig. 2(b). This spectrum contains a peak at zero energy associated with the ground state and a wider peak at ~ 1.7 MeV associated with the first excited state. For the ground-state peak, the solid curve in this figure shows the simulated spectrum, again including a background contribution (including a contribution from the first excited state), which is indicated by the short-dashed curve. The tabulated ^{6}Be mass excess and decay width were used in this simulation, which reproduces the experimental result very well, strongly suggesting that the disagreement of the simulation with the data for ^{8}C is not an experimental artifact. The experimental full width at half maximum of the ^{6}Be ground-state peak is 214 ± 10 keV, significantly greater than its intrinsic width of $\Gamma = 92 \pm 6$ keV. Thus the agreement between the ^{6}Be$_{g.s.}$ data and simulation indicates that we can correctly account for the experimental resolution.

The solid curve in Fig. 2(a) shows the results of a simulation where both the ^{8}C mass excess and its decay width were adjusted to best reproduce the experimental peak. The fitted mass excess is 35.030 ± 0.030 MeV and the fitted width is 130 ± 50 keV.

Previous measurements of the mass excess and decay width were made in Refs. [20–22] using transfer reactions. Of these, only the 1976 work of Tribble *et al.* [22] has more than a handful of ^{8}C events. The reaction studied was ^{12}C$(^4$He,^{8}He$)^8$C and the ^{8}He fragments were detected. The extracted mass excess was 35.10 ± 0.03 and the decay width was 230 ± 50 keV and 183 ± 56 keV assuming Breit-Wigner and Gaussian intrinsic lines shapes, respectively. As in the present work, the experimental resolution was significant.

The ^{8}C ground state is quite unusual in having a five-particle exit channel. It is of interest to determine whether this state disintegrates directly into five pieces or proceeds in a sequential process of two or more steps through intermediate states. Figure 3 shows the levels of possible interest in the decay. Of the possible intermediate states, the ^{6}Be ground state is the narrowest (longest lived) and easiest to detect experimentally. In each detected $4p + \alpha$ event, one can find six ways to reconstruct a ^{6}Be decay as a $2p + \alpha$ subset. For each of these ways, a ^{6}Be excitation energy is determined. We use gate $G1$ in Fig. 2(a) to select out the ground-state events. The resulting excitation-energy spectrum of all these potential ^{6}Be candidates is displayed in Fig. 4(a) as data points. As there can be at most only one ^{6}Be ground-state fragment per event, at least 5/6 of the spectrum corresponds to incorrectly reconstructed ^{6}Be fragments and these form a background. The experimental spectrum clearly displays a peak centered near zero energy associated with the ^{6}Be ground state on a background of approximately Gaussian shape.
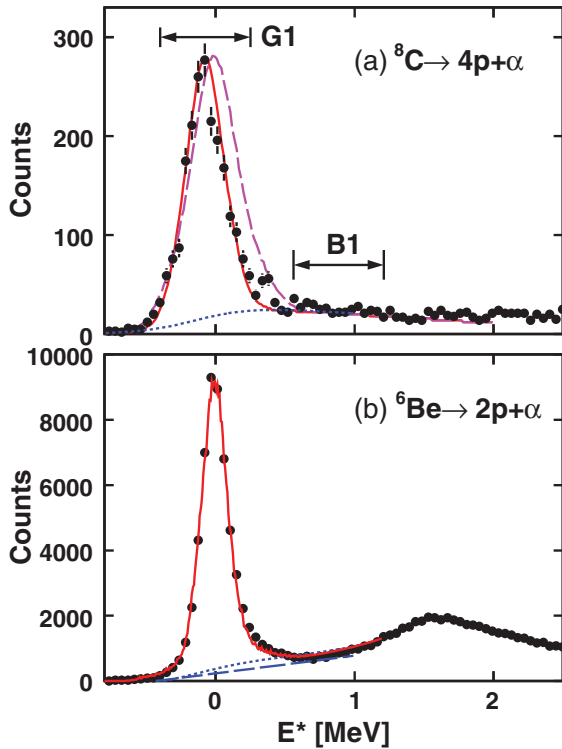
FIG. 2. (Color online) Excitation-energy spectra for (a) ^{8}C fragments produced in neutron knockout from the ^{9}C beam and (b) ^{6}Be fragments produced in neutron knockout from the ^{7}Be beam. In both cases, the curves show simulated ground-state distributions (see text). The solid curve in (a) is a fit to the data with a background indicated by the dotted curve. The dashed curve is the simulated response based on the tabulated peak location and width. The dotted and dashed curves in (b) show the two possible background distributions considered in the text.

To determine what fraction of the ^{8}C events decay through ^{6}Be$_{g.s.}$, we have fitted the spectrum in Fig. 4(a) with two components: a ^{6}Be$_{g.s.}$ component with shape taken from the experimental peak in Fig. 2(b) obtained with the ^{7}Be beam and a background component taken to be Gaussian in the immediate vicinity of the ^{6}B$_{g.s.}$ peak. In order to use the experimental ^{6}Be$_{g.s.}$ line shape from Fig. 2(b), one has to first subtract the small background under this peak.
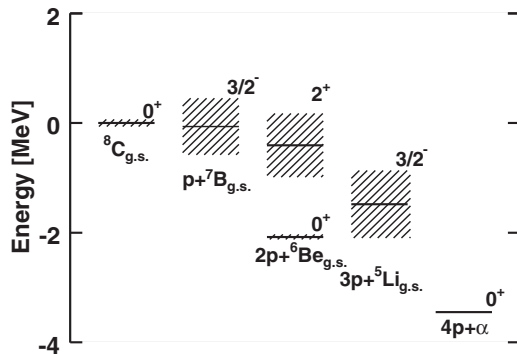
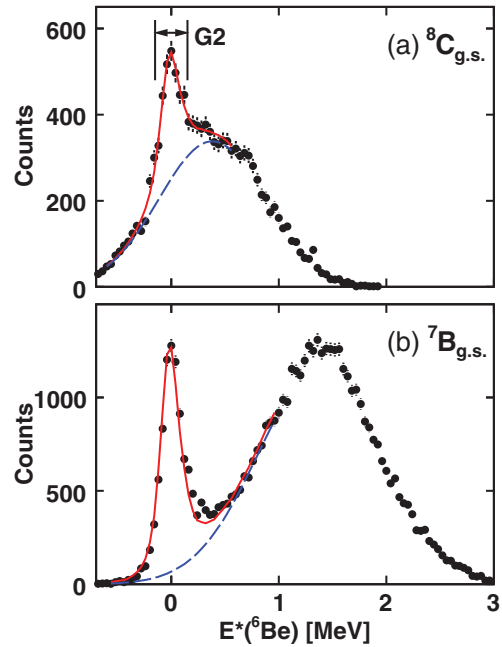FIG. 3. Levels of interest in the decay of the ^{8}C and ^{7}B ground states.

FIG. 4. (Color online) The spectrum of all possible reconstructed ^{6}Be excitation energies for events in the ground states of (a) ^{8}C and (b) ^{7}B. The data points are the experimental data, while the solid curves show fits to the ^{6}Be ground-state region with the dashed curves showing the fitted background.

The short- and long-dashed curves in this figure show two possible backgrounds which were considered. The short-dashed curve is associated with the solid curve obtained using a symmetric Breit-Wigner line shape. The use of the long-dashed background curve would imply a slightly asymmetric ^{6}Be$_{g.s.}$ line shape which has an enhanced higher-energy tail. A small degree of asymmetry is not unreasonable.

The resulting fit (using the original ^{6}Be background) is shown by the solid curve in Fig. 4(a) where the Gaussian background is indicated by the dashed curve. Taking into account both possible ^{6}Be backgrounds, these fits imply that, on average, 1.01 ± 0.05 ^{6}Be$_{g.s.}$ fragments are created in each ^{8}C$_{g.s.}$ decay, i.e., essentially all decays pass through ^{6}Be$_{g.s.}$. This number was corrected for the small background under the ^{8}C$_{g.s.}$ peak itself [dotted curve in Fig. 2(a)], using the region $B1$ to estimate the ^{6}Be probability associated with this background.

In many ways, the decay of ^{8}C$_{g.s}$ to $2p + {}^6$Be$_{g.s.}$ is similar to the decay of ^{6}Be$_{g.s.}$ to $2p + \alpha$. In each case, both the initial and final states are $J^\pi = 0^+$ and the possible intermediate states (^{7}B$_{g.s.}$ and ^{5}Li$_{g.s.}$) are $J^\pi = 3/2^-$. These intermediates states are both wide, but only their low-energy tails are energetically accessible. Both decays are democratic; $R_E = 1.2$ and 1.9 and $d_E = 8.8$ and 6.5 fm for ^{8}C and ^{6}Be, respectively. Thus the disintegration of ^{8}C$_{g.s.}$ is novel, having two sequential steps of democratic two-proton decay. To investigate this possibility, it is useful to separate out experimentally the protons from the first and second decay steps. However, it is not possible to do this with 100% certainty for all decays.

For a fraction of the events it is possible to make this separation with reasonable precision. To this end, we have

selected events where one, and only one, of the six possible reconstructed ^{6}Be fragments has an excitation energy associated with the ground-state peak indicated by the region $G2$ in Fig. 4(a). For the events which survive this criteria, the identities of the ^{6}Be$_{g.s.}$ decay products are obvious.

Some events from the tails of the ^{6}Be$_{g.s.}$ peak lie outside the $G2$ region and will be rejected. Also, and more importantly, one can have the situation that the correct ^{6}Be fragment is in the high- or low-energy tail outside of the gate and an incorrectly identified ^{6}Be fragment lies within the $G2$ gate. Such an event will not be rejected, but the identities of the protons from the first and second steps will be incorrect. Monte Carlo simulations were used to optimize the width of the $G2$ region so as to obtain the best compromise between event rejection and misidentification.

With the chosen gate width we select only 30% of the ^{8}C$_{g.s.}$ events and, of these, we estimate that a selected event is incorrectly identified 30% of the time. While this is significant, these misidentifications involve cases were the two protons assigned to one of the decay steps are actually from the two separate steps. As the two steps are separated by a ^{6}Be$_{g.s.}$ fragment with $J^\pi = 0^+$, there is no angular correlations between the protons from the two steps and these misidentified events will give rise only to smooth backgrounds in the correlation plots.

The energy and angular correlations between the particles produced in two-proton decay can be described by the hyperspherical Jacobi vectors **X** and **Y** and their conjugate momenta $\mathbf{k}_x$ and $\mathbf{k}_y$. There are two independent ways of defining the coordinates which are referred to as the "T" and "Y" systems. These are illustrated in Fig. 5 where the core (fragment 3 in the T system or fragment 2 in the Y system) is the ^{6}Be$_{g.s.}$ fragment in the first $2p$ decay and the α particle in the second $2p$ decay. In terms of the position vectors $\mathbf{r}_i$, momentum vectors $\mathbf{k}_i$, and masses m_i ($i = 1, 2$, and 3) the Jacobi coordinates are

$$\mathbf{X} = \mathbf{r}_1 - \mathbf{r}_2, \tag{17a}$$

$$\mathbf{Y} = \frac{m_1\mathbf{r}_1 + m_2\mathbf{r}_2}{m_1 + m_2} - \mathbf{r}_3, \tag{17b}$$

$$\mathbf{k}_x = \frac{m_2\mathbf{k}_1 - m_1\mathbf{k}_2}{m_1 + m_2}, \tag{17c}$$

$$\mathbf{k}_y = \frac{m_3(\mathbf{k}_1 + \mathbf{k}_2) - (m_1 + m_2)\mathbf{k}_3}{m_1 + m_2 + m_3}. \tag{17d}$$

Of the six degrees of freedom required to define the $\mathbf{k}_x$ and $\mathbf{k}_y$ distributions, three describe the Euler rotation of the decay plane and one is constrained from energy conservation. Thus the complete correlation information can be described by two variables which we take as E_x/E_T and θ_k, where E_x is the energy associated with the X coordinate,

$$E_x = \frac{(m_1 + m_2)k_x^2}{2m_1m_2}; \tag{18}$$

E_T is the total three-body energy and θ_k is the angle between the Jacobi momenta,

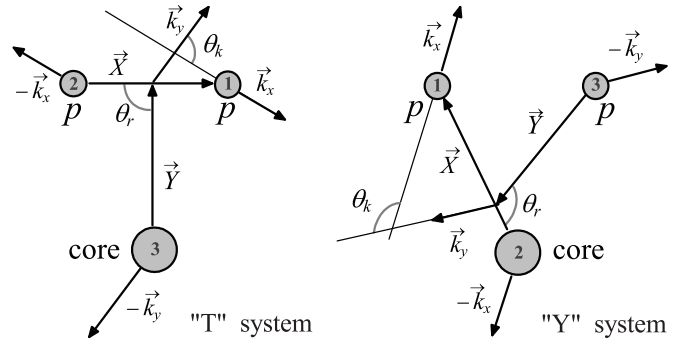$$\theta_k = \frac{\mathbf{k}_x \cdot \mathbf{k}_y}{k_x k_y}. \tag{19}$$

FIG. 5. Independent T and Y Jacobi systems for the core $+ N + N$ three-body system in coordinate and momentum spaces.

For each event, there are two ways of labeling the two protons and thus there are two possible values of the $[E_x/E_T, \cos(\theta_k)]$ coordinate, both of which are used to increment the correlation histograms. For the T system, this produces a symmetrization of the angular distributions about $\cos(\theta_k) = 0$.

Distributions constructed in the two Jacobi systems are just different representations of the same physical picture. Each Jacobi system can reveal different aspects of the correlations. The Jacobi Y system is particularly useful if the two protons are emitted sequentially through an intermediate state. In this case, E_x is the kinetic energy released in the second step and θ_k is the angle between the two decay axes. The Jacobi T system can have a similar interpretation for a diproton decay with an intermediate ^{2}He state.

The projected correlations in both the T and Y systems are plotted in Fig. 6 for the second decay step of ^{8}C$_{g.s.}$, i.e., the $2p$ decay of the ^{6}Be$_{g.s.}$ intermediate state. These can be compared to results from the ^{7}Be beam in Fig. 7, where ^{6}Be$_{g.s.}$ is formed more directly following a neutron-knockout reaction. In this case, the statistical uncertainties are significantly smaller and there are no misidentified events. A consistency between the projected correlations in Figs. 6 and 7 is necessary if the ^{8}C$_{g.s.}$ level disintegrates through ^{6}Be$_{g.s.}$ and indeed the corresponding projected correlations are quite similar in the two figures.

In order to make more detailed comparisons of the experimental ^{6}Be correlations in Figs. 6 and 7, we have made extensive Monte Carlo simulations, including the effect of the detector response and the event selection requirements. The results from the ^{7}Be beam in Fig. 7 are compared to simulations where the effect of the detector resolution and acceptance is considered with no misidentification or selection bias. The detector effects induce only small modifications to the projected correlations in this case. The solid curves are predicted distributions from the quantum-mechanical three-body cluster model of Ref. [6] (calculation P2 in that reference). This model reproduces the experimental total energy E_T, Γ, and the experimental correlations in Fig. 7. These predicted correlations will therefore be used in the simulations in the disintegration of ^{8}C.

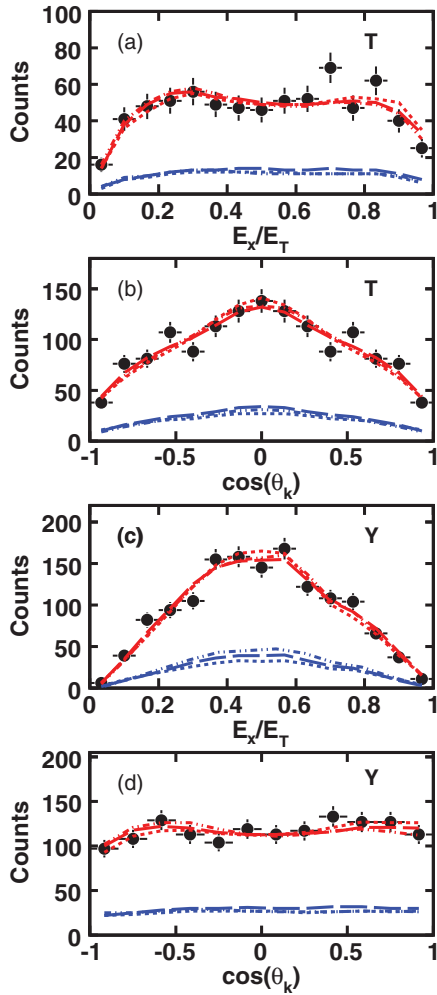The dashed curves in Fig. 7 are from an R-matrix approximation of sequential two-proton emission from ^{6}Be$_{g.s.}$

FIG. 6. (Color online) Projected correlations in (a),(b) T and (c),(d) Y Jacobi systems for the three-body decay of ^{6}Be formed in the second step of ^{8}C$_{g.s.}$ decay. Angular correlations are shown in (b) and (d) and energy correlations are shown in (a) and (c). The data points are the experimental data, while simulated results are indicated by the curves which pass through the data points. The lower curves are estimates of the "backgrounds" of incorrectly identified events. The short- and long-dashed and solid curves are associated with simulations (i), (ii), and (iii), respectively (see text).

FIG. 7. (Color online) As for Fig. 6, but now for ^{6}Be$_{g.s.}$ events produced via neutron knockout from the ^{7}Be beam. The solid and dashed curves show predictions of the three-body cluster model and a sequential-decay calculation, respectively.

through the ^{5}Li$_{g.s.}$ intermediate state as described in Sec. III. The angular correlations in this simulation are particularly strong and favor decays where the two sequential decay axes are collinear, i.e., $\cos(\theta_k) = \pm 1$ in the Jacobi Y system [see Fig. 7(d)]. This angular correlation is also responsible for the predicted broad minimum in the energy distribution in the Jacobi T system [Fig. 7(a)]. However, these features associated with the predicted angular correlation are lacking in the experimental data. This indicates that the decay of ^{6}Be$_{g.s.}$ does not pass through an intermediate state of well defined angular momentum ($J^\pi = 3/2^-$). Similar conclusions have been made in other studies of ^{6}Be$_{g.s.}$ [4,5].

Now let us return to ^{6}Be$_{g.s.}$ decay in the process of ^{8}C$_{g.s.}$ disintegration. In order to include the bias from the event selection and the contribution from misidentified events, it is necessary

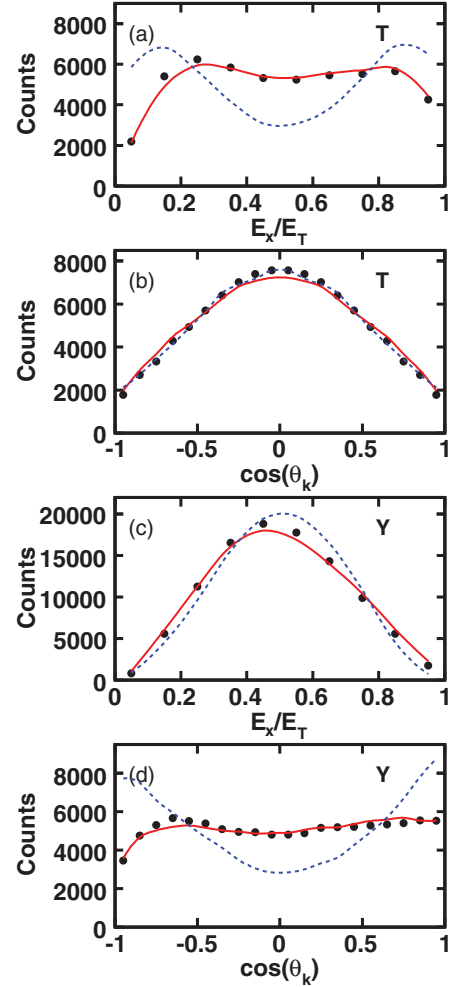to simulate the first step of ^{8}C$_{g.s.}$ disintegration. For this first decay step, ^{8}C $\to 2p + {}^6$Be$_{g.s.}$, we have considered three quite different sets of simulated $[E_x/E_t, \cos(\theta_k)]$ correlations:

(i) The momenta of the three fragments are chosen according to available phase-space volume.

(ii) The $[E_x/E_t, \cos(\theta_k)]$ correlations for the Jacobi T system is taken to be the same as for ^{6}Be$_{g.s.}$ decay. Note that as the core mass is different in the ^{8}C$_{g.s.}$ two-proton decay, the Jacobi-Y distribution will not be exactly the same as for ^{6}Be$_{g.s.}$ decay.

(iii) The decay is treated in the R-matrix approximation as a sequential two-proton decay through the ^{7}B intermediate state in a similar manner as just described for the sequential two-proton decay of ^{6}Be$_{g.s.}$. The R-matrix parameters for ^{7}B$_{g.s.}$ are taken from Sec. IV B.

The short-dashed, long-dashed, and solid curves in Fig. 6 are the results for ^{6}Be$_{g.s.}$ decay in the second step of ^{8}C$_{g.s.}$ disintegration for simulations (i), (ii), and (iii), respectively.

The curves, which pass through the data points in each panel, include the detector response, the selection bias, and the contribution from the incorrectly identified events. The latter contributions are indicated by the lower curves in each panel. In all cases, the three curves from the different simulations almost overlap. Thus the simulated results for $^6Be_{g.s.}$ decay show very little sensitively to the decay correlations in the first $^8C \rightarrow 2p + {}^6Be_{g.s.}$ step. Our assertion that the distributions for the misidentified events show no strong structure is borne out and the simulations for all selected events reproduce the experimental data. Therefore within the statistical errors on the experimental data and uncertainty associated with extracting the data, the correlations in the second step of ^8C disintegration are consistent with $^6Be_{g.s.}$ decay.

For the first step $(2p + {}^6Be_{g.s.})$ of $^8C_{g.s.}$ decay, the projected E_x/E_t and $\cos(\theta_k)$ distributions for both the Jacobi T and Y systems are plotted in Fig. 8. The curves in each panel show the simulated distributions and backgrounds from the three simulations discussed above. Again these backgrounds are similar in all the simulations and show relatively smooth behaviors. Clearly, the phase-space simulation (short-dashed curve) is inconsistent with all the experimental projected correlations. Also the simulations using the theoretical ^6Be correlations (long-dashed curves) do not fit the data in Figs. 8(a) and 8(d) indicating that two-proton correlations are different in the first and second steps.

The sequential decay simulations gives the best description to all the experimental distributions, however, it is clearly not perfect. The predicted angular correlations indicated by the solid curve in Fig. 8(d) show strong enhancements near $\cos(\theta_k) = \pm 1$. These angular correlations also cause the large structure predicted for the Jacobi T energy distribution of Fig. 8(a). The experimental data also show an enhancement near $\cos(\theta_k) = -1$, sometimes called the diproton region, however, the corresponding enhancement near $\cos(\theta) = 1$ is not evident. In the sequential scenario, $\cos(\theta) = 1$ corresponds to the ^6Be core from the second step being directed toward the proton from the first step. Coulomb final-state interactions may deflect the trajectories and thus suppress the yield near $\cos(\theta) = 1$. Alternatively the enhancement near $\cos(\theta_k) = -1$ may not be related to a sequential angular correlation but rather might be a signature of some "diproton" character of the decay similar to that observed for the 6.57-MeV state in ^{10}C [23].

The total decay width in the sequential scenario can be estimated as [14,15]

$$\Gamma^0 = \frac{\Gamma_{tot}(Q_1)}{1 + \gamma_1^2 \int_0^\infty \left(\frac{dS_{1\ell}(E_T - E_x)}{dE_x} \right)_{Ex=Q_1} \rho(E_x) dE_x}. \quad (20)$$

The $p + {}^7B_{g.s.}$ spectroscopic factor was calculated with Cohen-Kurath interaction (CKI) Hamiltonian [24] as $S = 3.20$ $(8/7)$ where $(8/7)$ is the center-of-mass correction. With $\theta_{sp}^2 = 0.44$ from Eq. (16) we estimate $\gamma_1^2 = 4.28$ MeV and thus $\Gamma^0 = 12$ keV, which is significantly less than the experimental value of 130 ± 50 keV and thus it is clear that this sequential decay scenario cannot provide a total description of the two-proton decay of $^8C_{g.s.}$.

Given the enhanced "diproton" character of the decay it is useful to consider the diproton decay model, which can be
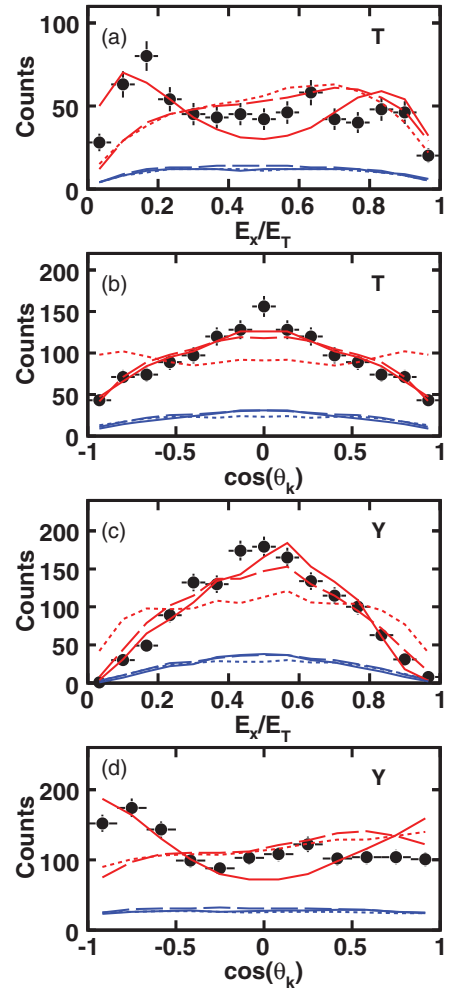

FIG. 8. (Color online) As for Fig. 6, but now the correlations are associated with the first step of $^8C_{g.s.}$ decay forming $2p + {}^6Be_{g.s.}$.

treated in the R-matrix formulation of Barker [25] together with the diproton cluster decay model developed in Ref. [26]. For the wave functions we use the p-shell basis with the CKI Hamiltonian [24].

The diproton decay spectroscopic factor is given as a product of the three terms as in Eq. (7) of [26]. For the ^8C decay these are $(8/6)^2 = 1.78$ (the center-of-mass correction), $G^2(p) = 1/2$ (the cluster overlap factor) and $C = 1.21$ (the p-shell spectroscopic factor for $L = S = 0$), to give $S_{62} = 1.08$. The related single-particle dimensionless reduced width of $\theta_{sp}^2 = 1.00$ is also taken from Ref. [25]. The diproton decay width obtained for the experimental decay energy of $Q_1 = 2.077$ MeV is $\Gamma = 88$ keV. If we use the older Q_1 value of 2.147 MeV based on the tabulated masses, the width would be 100 keV. We have assumed a narrow ^6Be final state. The change coming from a folding with its actual width is small. Our spectroscopic factor S_{62} is a factor of five larger than given by Barker following Eq. (13) of Ref. [25]. We do not know why, but assume that there was an error in Barker's calculation.

The calculated diproton decay width of $\Gamma = 88$ keV is consistent with the experimental value of 130 ± 50 keV, supporting the interpretation of the enhancement at low E_x/E_T

in the Jacobi T system [Fig. 8(a)] as a diproton feature. However, the diproton model does not provide a complete description of the experimental correlations. For example, in the diproton model, the Jacobi T angular distribution is just the distribution of the diproton decay angle, which should be isotropic as the diproton has $J^\pi = 0^+$. However, the experimental distribution in Fig. 8(b) is not uniform and thus inconsistent with this notion.

We have also considered the diproton model for $^6\text{Be}_{g.s.}$ decay. For the spectroscopic factor we obtain $(6/4)^2 = 2.25$ (the center-of-mass correction), $G^2(p) = 1/2$ (the cluster overlap factor) and $C = 1.00$ (the p-shell spectroscopic factor for $L = S = 0$), to give $S_{42} = 1.12$. With the single-particle dimensionless reduced width of $\theta_{sp}^2 = 1.13$ [25], the diproton decay width obtained for $Q_1 = 1.371$ MeV is $\Gamma = 98$ keV again consistent with the tabulated value of 92 ± 6 keV. However, in this case the diproton nature of the experimental correlations (Fig. 7) is even less apparent. Clearly a complete understanding of $^6\text{Be}_{g.s.}$ and $^8\text{C}_{g.s.}$ requires a full three-body decay calculation.

B. ^{7}B levels

The ^{7}B excitation-energy spectrum determined from all detected $3p + \alpha$ events is displayed in Fig. 9(a). The peak near zero excitation energy indicates that the ground state of ^{7}B was produced in the reaction. There is a significant contamination in this spectrum from $^8\text{C}_{g.s.}$ disintegrations where only three of the four protons were detected. To determine the contribution from this process, we have taken detected $4p + \alpha$ events associated with $^8\text{C}_{g.s.}$ and generated pseudo $3p + \alpha$ events by alternatively removing one of the protons and determined the ^{7}B excitation energy. The distribution of these excitation energies is labeled as $^8\text{C}_{g.s.}$ in Fig. 9(a) and indicates that the incompletely detected $^8\text{C}_{g.s.}$ events lead to an enhancement of the low-energy side of the $^7\text{B}_{g.s.}$ peak. The Monte Carlo simulations were used to normalize the $^8\text{C}_{g.s.}$ distribution to the expected number of incomplete detected events. The data points in Fig. 9(b) show the results for the ^{7}B excitation-energy spectrum after this $^8\text{C}_{g.s.}$ contamination was subtracted.

The subtracted distribution peaks at $E^* \sim -100$ keV rather than zero, suggesting that the evaluated mass excess from Ref. [19] used to calculate the Q value for this figure is incorrect. This evaluated mass excess of 27.94 ± 0.10 MeV was derived from an average of two measurements; 27.80 ± 0.10 MeV from the $^7\text{Li}(\pi^+,\pi^-)^7\text{B}$ reaction and 27.94 ± 0.10 MeV from the $^{10}\text{B}(^3\text{He},^6\text{He})^7\text{B}$ reaction [27].

As this is a rather wide level near threshold, the use of a Breit-Wigner line shape may not be appropriate. We have used R-matrix theory [14] assuming $p + ^6\text{Be}_{g.s.}$ as the only open decay channel. The line shape is given by Eq. (8) where now E_x is the energy above the $p + ^6\text{Be}_{g.s.}$ threshold, and Q_2 is the resonance energy. Using $J^\pi = 3/2^-$ listed in the ENSDF database and $\ell = 1$, the experimental spectrum was fit by adjusting E_2 and γ_2^2 and other parameters defining a smooth background under the peak. The effects of the detector acceptance and resolution was taken into account via the Monte Carlo simulations. The resulting fit is displayed as the
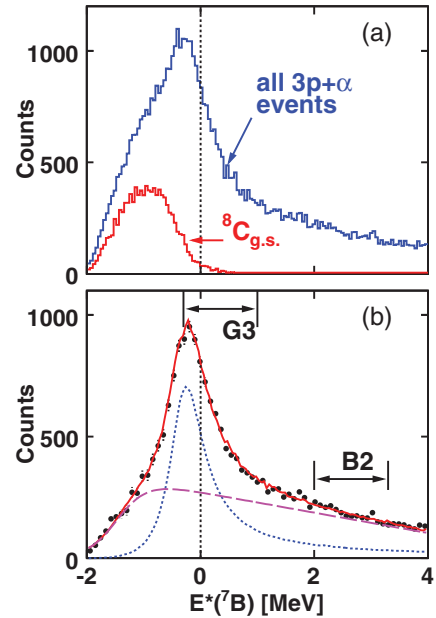

FIG. 9. (Color online) (a) The excitation-energy spectra for ^{7}B events determined from all detected $3p + \alpha$ events and from $^8\text{C}_{g.s.}$ $4p + \alpha$ events where one of the protons was ignored. (b) The data points are the ^{7}B excitation-energy spectrum after the ^{8}C contamination was subtracted. The solid curve shows a fit to these data assuming an R-matrix line shape and including the detector response. The long-dashed curves indicate the background obtained from the fit and the raw R-matrix line shape is indicated by the dotted curve.

solid curve in Fig. 9(b) and the fitted background is shown as the dashed curve. The dotted curve shows the fitted peak shape without the effects of the detector acceptance and resolution.

The fitted resonance energy is $Q_2 = 2.013 \pm 0.025$ MeV, which implies a mass excess of 27.677 ± 0.025 MeV. The error includes the effect in a 20% uncertainty in the magnitude of the subtracted ^{8}C contamination. This mass excess is consistent with the previous measurement from the $^7\text{Li}(\pi^+,\pi^-)^7\text{B}$ reaction, but is inconsistent with that from the $^{10}\text{B}(^3\text{He},^6\text{He})^7\text{B}$ reaction. The fitted reduced width is $\gamma_2^2 = 1.32 \pm 0.02$ MeV and thus the level width [14],

$$\Gamma^0 = \frac{\Gamma(Q_2)}{1 + \gamma_2^2 \left(\frac{dS_\ell}{dE_x}\right)_{E_x = Q_2}}, \tag{21}$$

is 0.80 ± 0.02 MeV. The evaluated width in the ENDSF database is 1.4 ± 0.2 MeV derived from the $^{10}\text{B}(^3\text{He},^6\text{He})^7\text{B}$ reaction [27]. Again our results are inconsistent with this measurement.

In the above analysis of this level, we assumed $^7\text{B}_{g.s.} \rightarrow p + ^6\text{Be}_{g.s.}$ sequential decay. We can check this by looking for a $^6\text{Be}_{g.s.}$ fragment as described in Sec. IV A. Here, there are only three ways to reconstruct a ^{6}Be fragment from three protons and an α particle. The distribution of all three possible ^{6}Be excitation energies is shown in Fig. 4(b) for the gate $G3$ in Fig. 9(b) on the ^{7}B excitation energy. This gate does not cover the whole of the $^7\text{B}_{g.s.}$ peak width, but avoids the lower energies where the ^{8}C contamination is present. The ^{6}Be excitation-energy spectrum displays a prominent peak

at zero excitation energy indicating that ^{6}Be$_{g.s.}$ fragments were produced in the decay. The solid curve shows a fit to the data using the experimental ^{6}Be$_{g.s.}$ line shape [Fig. 2(b)] and a smooth Gaussian background (dashed curve) under this peak. From this fit we determine that, on average, there is a $54 \pm 6\%$ probability of finding a ^{6}Be$_{g.s.}$ fragment in the $G3$ gate. However, it is clear from Fig. 9(b) that there is a very significant background under this peak. Using gate $B2$ in Fig. 9(b) we estimate that the background has a $19 \pm 2\%$ probability of containing a ^{6}Be$_{g.s.}$ fragment. Using this, we find that $81 \pm 10\%$ of the ^{7}B$_{g.s.}$ events decay via $p + {}^6$Be$_{g.s.}$.

Shell-model calculations for ^{7}B$_{g.s.}$ with the CKI Hamiltonian [24] give the spectroscopic factor for the $p + {}^6$Be$_{g.s.}$ configuration as $S = 0.59(7/6) = 0.688$. The $p + {}^6$Be$_{1.67}(2^+)$ configuration is predicted to be $\sim$3 times stronger but decay to this channel is suppressed due to its significantly smaller barrier penetration factor. With $\theta_{sp}^2 = 0.688$ from Eq. (15), this gives us a predicted reduced width of 1.42 MeV [Eq. (16)]. Taking into account the 81% branching ratio, we estimate the experimental value to be $\gamma^2 = 1.07 \pm 0.15$ MeV, which is quite similar to the predicted value, confirming that the $p + {}^6$B$_{g.s.}$ is not the strongest configuration in ^{7}B$_{g.s.}$.

Although it is possible to consider a proton decay through the 1.670-MeV ($J^\pi = 2^+$) first-excited state of ^{6}Be (see Fig. 3), this ^{6}Be intermediate state is sufficiently wide that the disintegration is democratic. The average energy released in the first step is $E_k = 343$ keV (determined from the differences in centroids of the two levels), which is very small compared to the width of the intermediate state, $\Gamma = 1.16$ MeV. Alternatively, the distance traveled by the proton on average before the ^{6}Be fragment decays is 2.0 fm, which is small compared to the nuclear diameter. Thus this decay strength is probably best described as a four-body decay.

C. ^{8}B levels

The ^{8}B excited states studied in this work and their observed decay paths are illustrated in the level diagram of Fig. 10. We observed excited states in three detected exit channels; $p + {}^3$He $+ \alpha$, $2p + {}^6$Li, and $2p + d + \alpha$. The $p + {}^7$Be channel, which is probably the most important exit channel for many states, was not accessible in this work, as Be fragments saturate the Si shaping amplifiers.

1. $p + {}^3$He $+ \alpha$ exit channel

The ^{8}B excitation-energy spectrum derived from all detected $p + {}^3$He $+ \alpha$ events, shown in Fig. 11(a), displays wide peaks at 5.93 and 8.15 MeV. The ^{7}Be excitation-energy distribution obtained from the ^{3}He $+ \alpha$ pairs associated with each of these events is shown in Fig. 11(b). A peak associated with the 4.57-MeV $7/2^-$ level is prominent. The total ^{8}B excitation spectra is subdivided in Fig. 11(a) into those in coincidence with the ^{7}Be peak [gate $G4$ in Fig. 11(b)] and those that are not. This subdivision separates the two ^{8}B peaks. The 5.93-MeV peak is associated with proton decay to the 4.57-MeV state of ^{7}Be and 8.15-MeV state does not decay by this path. Let us first concentrate on the 5.93-MeV peak.
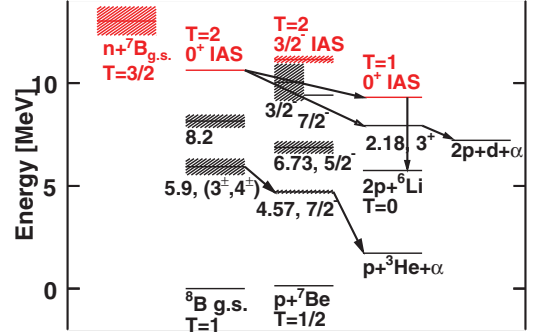

FIG. 10. (Color online) Level scheme showing the levels of ^{8}B discussed in this work and their decay paths.

As there are only three fragments in the exit channel, the velocity vectors of the decay products are located in a plane in the ^{8}B center-of-mass frame. To display the correlations between the decay fragments, we have projected these vectors onto that plane, and then within this plane, rotated all the vectors such that the locations of all the α-particle velocities approximately coincide and at the same time the locations of all the ^{3}He fragments' velocities approximately coincide. This was achieved by requiring that the relative ^{3}He-α velocity was parallel to the V_z axis. A contour plot of the resulting distribution of p, ^{3}He, and α velocities is displayed in Fig. 12. The ^{3}He-α separation is constant as these fragments come from the decay of the 4.57-MeV ^{7}Be state. The protons lie approximately on an arc centered at the origin (^{8}B center of mass), as indicated by the dashed curve. Clearly the protons were emitted in the first step and the magnitude of their velocity is independent of their emission direction and the subsequent decay axis of the ^{7}Be intermediate state.

The decay of this state is expected to be sequential with $R_E = 0.11$ and $d_E = 60$ fm, and thus the two decay steps are largely independent, apart from consideration of conservation laws. Angular momentum conservation gives rise to the angular correlations. Let us consider the relative angle θ_{12} between the two decay steps, which is related to the angle θ_k in the Jacobi Y system. A $\theta_{12} = 0$ corresponds to an event where the proton in the first step and the α in the second step are emitted in the same direction. The distribution of θ_{12} is shown as the data points in both panels of Fig. 13. The experimental distribution is symmetric about $\cos(\theta_{12}) = 0$ consistent with the expectation for a sequential decay scenario. The experimental distribution is clearly not isotropic (flat). The predicted correlations in a sequential decay depend on the initial spin J and the total angular momentum removed by the proton j_p in the first decay step. The predicted correlations do not depend on the parity of the initial state for these proton decays, but mixing between j_p values should also be considered, i.e., the angular correlation becomes

$$w(\theta_{12}) = |\alpha_1|^2 w_1(\theta_{12}) + |\alpha_2|^2 w_2(\theta_{12})$$
$$+ (\alpha_1 \alpha_2^* + \alpha_1^* \alpha_2) w_{inter}(\theta_{12}), \quad (22)$$

where w_1 and w_2 are the correlations associated with two pure values of j_p, α_1 and α_2 are their complex amplitudes and w_{inter} is the interference term.
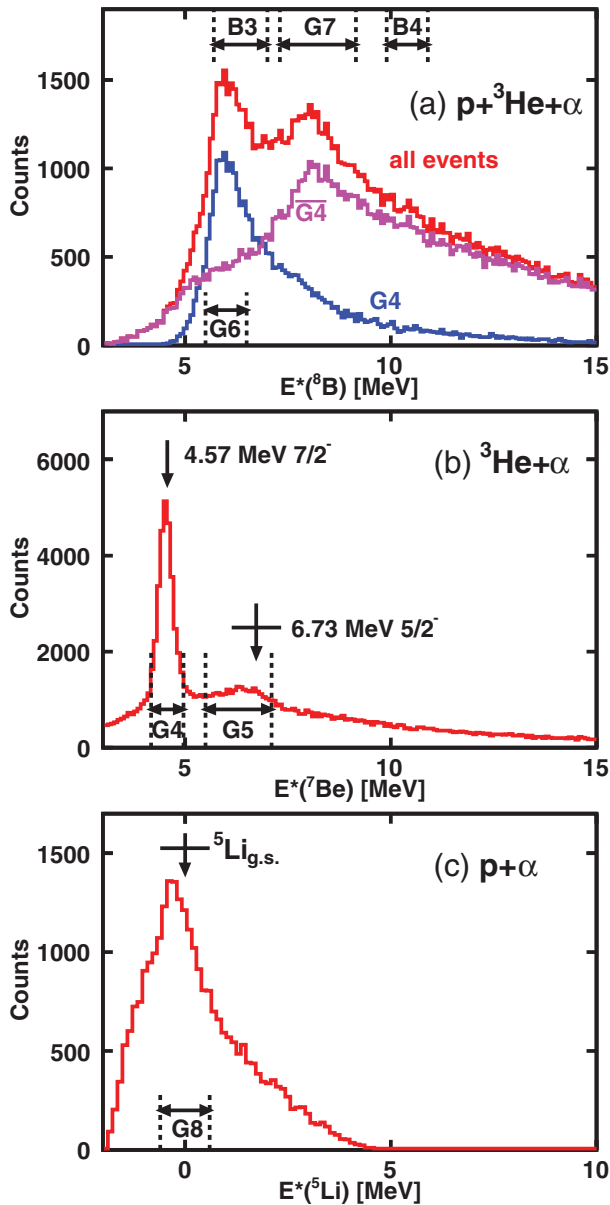
FIG. 11. (Color online) Excitation-energy spectra determined from $p + {}^3\mathrm{He} + \alpha$ events. (a) The ${}^8\mathrm{B}$ excitation spectrum from all $p + {}^3\mathrm{He} + \alpha$ events and its decomposition into those associated with the 4.57-MeV ${}^7\mathrm{Be}$ intermediate state and those not. (b) The ${}^7\mathrm{Be}$ excitation spectrum obtained from the ${}^3\mathrm{He}$-α pairs of all $p + {}^3\mathrm{He} + \alpha$ events. (c) Background-subtracted ${}^5\mathrm{Li}$ excitation-energy spectrum associated with the 8.15-MeV state in ${}^8\mathrm{B}$. Vertical arrows locate known levels with their widths indicated by the error bars. The gates used in this work are also indicated by the dashed lines.

With this mixing, only two possible J values were consistent with the experimental distributions. Figure 13(a) shows the results for $J = 3$. The two solid curves show the predictions for two pure values of j_p; 1/2 and 3/2. These predictions have been normalized to the same number of events as in the experimental distribution and Monte Carlo simulations indicate that the distortions due to the angular acceptance and energy resolution of the detectors are minimal. Neither of these predictions fit the data at all. However, a mixed solution with
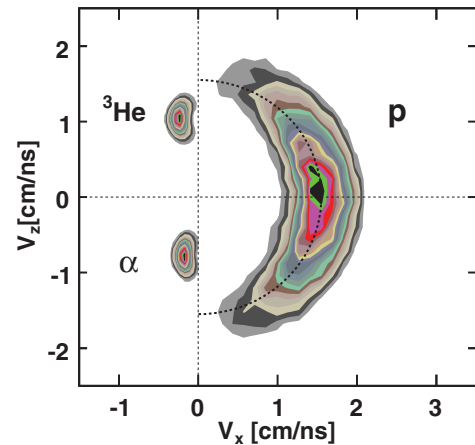

FIG. 12. (Color online) Distributions of velocities of the three fragments for the $p + {}^3\mathrm{He} + \alpha$ exit channel associated with the 5.93-MeV ${}^8\mathrm{B}$ state. Events were selected using the $G4$ and $G6$ gates in Fig. 11. The distributions are projected onto the plane of the decay, with all ${}^3\mathrm{He}$ and all α-particles' locations forced to be approximately coincident.

relative amplitudes of $\alpha_1 = 1$ and $\alpha_2 = 0.49 \pm 0.14$ for the two j_p values, respectively, fits the data very well [dashed curve in Fig. 13(a)].

The other solution was obtained for $J = 4$ and is shown in Fig. 13(b). Again, pure $j_p = 1/2$ and 3/2 predictions are shown by the solid curves. In this case the $j_p = 3/2$ predictions fits the data reasonably well. If we allow for mixing, the best
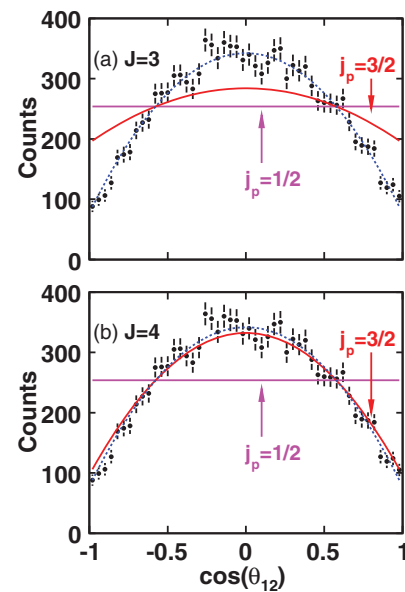

FIG. 13. (Color online) Angular correlations for the 5.93-MeV state of ${}^8\mathrm{B}$. Events were selected using both the $G4$ and $G6$ gates in Fig. 11. The angle θ_{12} is the relative angle between the initial proton decay axis and the subsequent ${}^3\mathrm{He}$-α decay axis in the ${}^8\mathrm{B}$ center-of-mass frame. The proton and α particle are emitted in the same direction when $\theta_{12} = 0$. The solid curves are predictions for pure values of j_p, while the dashed curves are for mixed values where the degree of mixing was chosen to best fit the data.

fit is obtained with relative amplitudes of $\alpha_2 = 1$ and $\alpha_1 = -0.07 \pm 0.10$, however, the level of mixing is minimal. All told, the angular correlations indicate that the 5.91-MeV state is either $J = 3$ or 4.

For the 8.15 MeV state in ^{8}B, which does not proton decay to the 4.57-MeV ^{7}Be state [Fig. 11(a)], it is difficult to clearly define its decay path due to the larger background under this peak and also because there are no possible narrow intermediate states through which it can decay. Sequential decay through a higher-lying ^{7}Be state and through the ^{5}Li ground state are possible. Apart from the narrow 4.57-MeV state, the ^{7}Be excitation spectra in Fig. 11(b) shows a broad peak at ∼6.5 MeV, close to the location of the $E^* = 6.73$-MeV, $J^\pi = 5/2^-$, $\Gamma = 1.2$-MeV state in ^{7}Be, indicated by the arrow in Fig. 11(b). For a wide intermediate state, the full width of the state is not always populated by sequential decay, as the Coulomb barrier of the first step can suppress the higher excitation region. The peak at 6.5 MeV may be associated with the 6.73-MeV state and gating of this peak enhances the 8.15-MeV peak. However, for all the $p + {}^3\text{He} + \alpha$ events, only $30 \pm 6\%$ of the kinetic energy, in the reconstructed ^{8}B frame, is associated with the proton. Thus the $^3\text{He} + \alpha$ pair accounts for the remaining $70 \pm 6\%$ and thus the ^{3}He-α reconstructed excitation energy is strongly correlated to $p + {}^3\text{He} + \alpha$ excitation energy suggesting that the 6.5-MeV peak in ^{7}Be spectra in Fig. 11(b) is a reflection of the peak at 8.15 MeV in Fig. 11(a) due to this strong correlation and not associated with an intermediate state.

Also possible is the decay $^8\text{B}^* \rightarrow {}^3\text{He} + {}^5\text{Li}_{g.s.}$. Figure 11(c) shows the reconstructed ^{5}Li excitation-energy spectrum determined for the p-α pairs associated with the 8.15-MeV peak [gate $G7$ in Fig. 11(a)]. A rough background correction was made using gates $B3$ and $B4$ on either side of the 8.15-MeV peak. A broad peak at zero excitation energy is observed overlapping strongly with the ground state of ^{5}Li. Angular correlations were constructed for both sequential decay scenarios, and after background subtractions, are shown in Fig. 14. In this figure $\theta_{12} = 0$ for $^3\text{He} + {}^5\text{Li}_{g.s.}$ decay corresponds to the ^{3}He and α being emitted in the same direction. The ^{3}He-^{5}Li$_{g.s.}$ result is clearly asymmetric about $\cos(\theta_{12}) = 0$ and cannot be explained by sequential decay. For the $p + {}^7\text{Be}_{6.73}$ case, although the distribution is symmetric about $\cos(\theta_{12}) = 0$, we were unable to fit it with the range of possible correlations expected for a $5/2^-$ intermediate state and thus there is no evidence for a sequential decay of this state, which suggests the decay is three body in nature.

2. $2p + {}^6$Li exit channel

The excitation-energy spectrum derived from $2p + {}^6$Li events in Fig. 15 displays a very prominent peak at 7.06 ± 0.02 MeV. The excitation energy in Fig. 15 was calculated based on the assumption that the ^{6}Li fragments were created in their ground states and did not γ decay. Only one ^{6}Li excited state has a significant γ-decay branch, the 3.562-MeV, $J^\pi = 0^+$, $T = 1$ level whose γ branching ratio is practically 100%. Therefore the peak observed in Fig. 15 can correspond
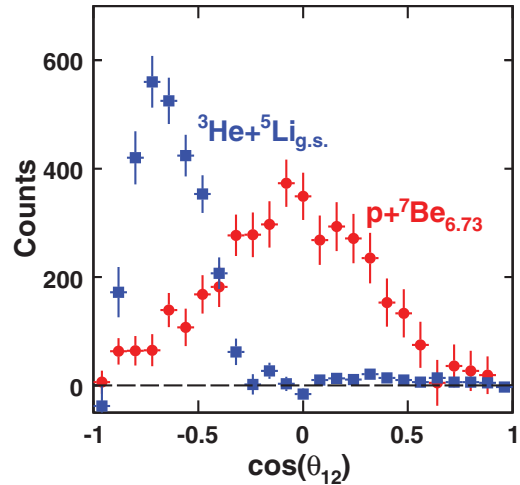

FIG. 14. (Color online) Background-subtracted angular correlations associated with possible sequential-decay scenarios for the 8.15-MeV state of ^{8}B. The 8-15-MeV peak was selected with gate $G7$ in Fig. 11 and the background was estimated from $B3 \cup B4$. For proton decay to the 6.73-MeV state of ^{7}Be, the extra gate $G5$ was applied and for ^{3}He decay to the ground state of ^{5}Li, the extra gate $G8$ was applied.

to a level of excitation energy of either 7.06 ± 0.02 or 10.62 ± 0.02 MeV.

The intrinsic width of this level is quite narrow, as the experimental width is similar to the predicted instrumental resolution. If we assume a Breit-Wigner line shape, we can further constrain the width. The curves in Fig. 15 show Monte Carlo predictions including the detector response for intrinsic widths of 50, 75, and 100 keV normalized to the experimental peak height. The behavior in the region of the low-energy tail, where the uncertainty due to the background contribution is minimal, suggests an intrinsic width of less than 75 keV.

There are no previously known levels at $E^* = 7.06$ MeV. From the mirror nucleus ^{8}Li, we expect only one narrow state near this energy, the mirror of the 6.53-MeV $J^\pi = 4^+$,
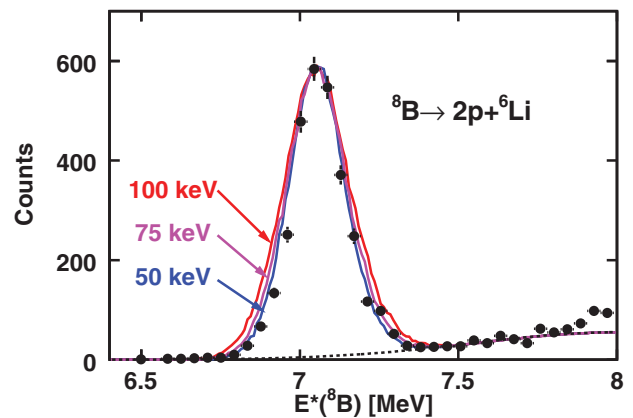

FIG. 15. (Color online) Excitation-energy spectra from $2p + {}^6$Li events. The curves show simulated distributions for Breit-Wigner line shapes with the indicated decay widths. The lower curve below the data indicates the background, which was included in the simulated distributions.

$\Gamma = 35$ keV level. However, this ^{8}Li state has a significant branch to the $n + t + \alpha$ exit channel passing through the 4.63-MeV ^{7}Li [28]. As the 7.06-MeV state is not observed in the mirror exit channel $p + {}^3\text{He} + \alpha$ (see Fig. 11) it seems unlikely that it can be this $J^\pi = 4^+$ state.

On the other hand, if the peak in Fig. 15 corresponds to a 10.62-MeV state, then we can immediately identify it with the known isobaric analog state (IAS) at $E^* = 10.619 \pm 0.009$ MeV, $J^\pi = 0^+$, $T = 2$, and $\Gamma < 60$ keV [29]. The almost exact matching of the excitation energy and a consistent limit to the width strongly support this assignment.

With this assignment, the ^{8}B state is thus the isobaric analog of $^8\text{C}_{g.s.}$ discussed in Sec. IV A and its structure should be similar. It decays by the emission of two protons to the isobaric analog of $^6\text{Be}_{g.s.}$ in ^{6}Li. Such a decay can conserve isospin only if the two protons are emitted promptly in a $T = 1$ configuration. Sequential two-proton decay does not conserve isospin as there are no energetically accessible $T = 3/2$ states available in the ^{7}Be intermediate nucleus (see Fig. 10). This is an isospin equivalent to the Goldansky two-proton decay, as the isospin allowed intermediate state is energetically forbidden.

Further elucidation of the nature of this two-proton decay may be obtained from the correlations between the fragments. Unfortunately in this experiment, most ^{6}Li fragments were not identified due to a saturation of the Si amplifiers, thus most of the $2p + {}^6$Li events associated with this state were not observed except where the ^{6}Li fragment had high kinetic energy (low ΔE) strongly biasing any correlation measurement. A future experiment is planned to study these correlations.

3. $2p + d + \alpha$ exit channel

The isobaric analog of the $^8\text{C}_{g.s.}$ state in ^{8}B also decays to the $2p + d + \alpha$ exit channel. Here, the decay is isospin forbidden and the yield is much smaller than that obtained for the $2p + {}^6$Li channel (Table I), further suggesting that the latter is an isospin-allowed decay. The excitation-energy spectrum extracted from these events is plotted in Fig. 16(a) and shows a narrow peak at the energy of the isobaric analog state (arrow). Possible narrow intermediate states are the ^{6}Be ground state and the 2.18-MeV $J^\pi = 3^+$ ^{6}Li excited state, although we found no evidence that the former is associated with this peak and in fact used the ^{6}Be ground state as a veto to reduce the background. The background was also reduced by gating on the reconstructed ^{8}B velocity distribution associated with the IAS peak for the $2p + {}^6$Li events. The spectrum labeled "all events" contained these two background reducing gates. For "all events," the reconstructed ^{6}Li excitation spectra from the d-α pairs is shown in Fig. 16(b) where the 2.18-MeV state is quite prominent. Gating on this state [gate $G4$ in Fig. 11(b)] produces the excitation-energy spectrum shown in Fig. 16(a). The peak in this case contains only $\sim$50% of the strength of the "all events" peak. The origin of the remaining strength is not clear, possibly from three or four-body decays, but certainly is not associated with sequential decay through a narrow state.

For the strength associated with the 2.18-MeV ^{6}Li state, we were not able to identify any ^{7}Be intermediate levels. Either the two protons are emitted in an initial three-body decay or the

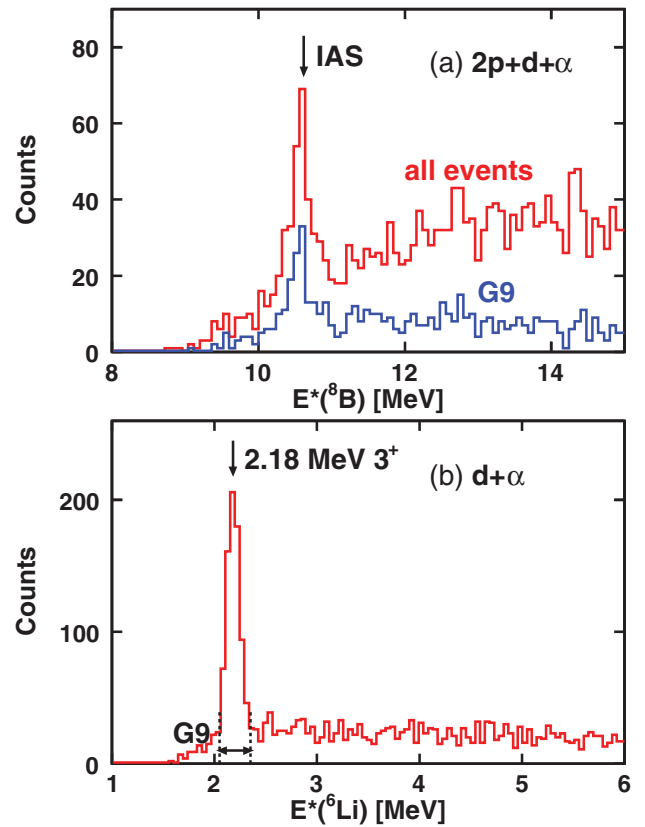FIG. 16. (Color online) (a) ^{8}B excitation-energy spectra obtained from $2p + d + \alpha$ events. (b) ^{6}Li excitation-energy spectrum obtained from each d-α pair of each $2p + d + \alpha$ event. The arrows indicate the locations of known states. The gate $G9$ in (b) is used to gate the spectrum in (a).

^{7}Be intermediate state(s) are too wide to isolate experimentally. Because of the low yields, the statistical errors associated with the background-subtracted correlations are too large to extract any further information.

D. ^{8}Be levels

A high-lying ^{8}Be state is seen in the $p + t + \alpha$ excitation spectrum. The distribution from all detected events is displayed in Fig. 17(a) ("all events"). A broad peak is observed at 22.96 MeV. Such a peak was also observed previously following the fragmentation of a ^{12}Be beam and was associated with proton decay to the 4.63-MeV $J^\pi = 7/2^-$ ^{7}Li excited state [13]. This is confirmed in the present work. The excitation spectrum obtained from the t-α pairs is shown in Fig. 17(b) where the 4.63-MeV ^{7}Li state is quite prominent. Gating on this peak [gate $G10$ in Fig. 17(b)] produced the "$G10$" spectrum in Fig. 17(a). The gate significantly reduced the background, but did not reduce the yield in the peak, indicating that proton decay to the 4.63-MeV state is the dominant decay mode.

This state has similarities to the 5.93-MeV state in ^{8}B which proton decays to the 4.57-MeV state in ^{7}Be, i.e., the mirror state to the 4.63-MeV in ^{7}Li. Figure 18 compares the angular distributions of θ_{12} in the decay of these two states. Here the
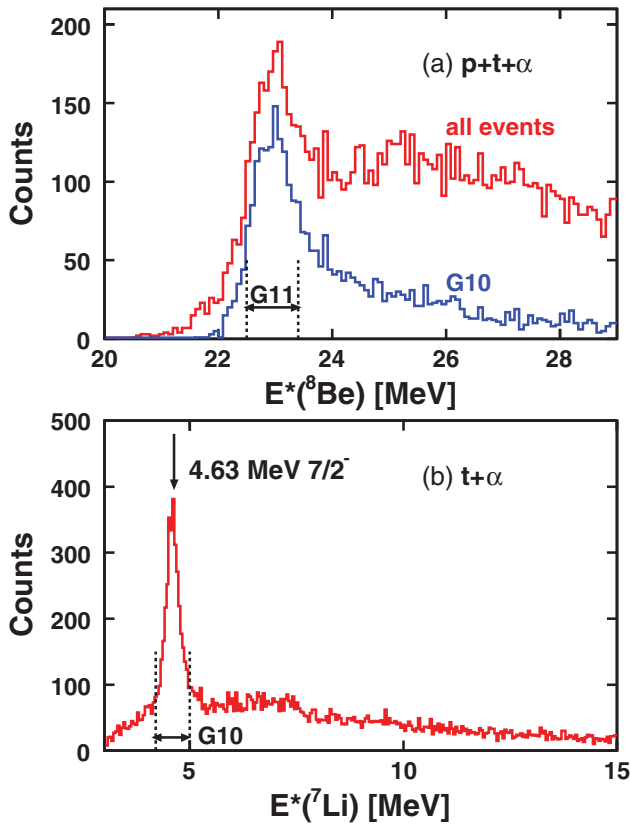
FIG. 17. (Color online) (a) ^{8}Be excitation-energy spectra from $p + t + \alpha$ events. (b) ^{7}Li excitation-energy spectrum from the t-α pairs in each $p + t + \alpha$ event.

^{7}B data were scaled to the same number of total counts as the ^{7}Be results. Within the statistical errors, the correlations are identical suggesting that the 22.96-MeV state in ^{8}Be is the analog of the 5.93-MeV ^{8}B state and thus would have the same possible spin assignments ($J = 3$ or 4). The intrinsic widths of these two states are also comparable: 850 ± 260 and 680 ± 146 keV for ^{8}B and ^{8}Be, respectively.

In Fig. 19 we show these levels in an isobar diagram of $T = 1$ levels. The relative excitation energies of these two levels is also consistent with their assignment to the same isospin triplet. The corresponding analog in the ^{8}Li nucleus is not entirely clear. A 6.1-MeV ^{8}Li state with $\Gamma \sim 1$ MeV is a possibility; it has been tentatively assigned $J = 3$.

E. ^{9}B

We observed ^{9}B levels in the $p + 2\alpha$ and $2p + {}^7$Li exit channels. Figure 20 shows a level diagram with the levels of interest and their decay paths.

1. $p + 2\alpha$ exit channel

The ^{9}B excitation-energy spectrum derived from $p + 2\alpha$ events, displayed in Fig. 21(a), shows many peaks. The most prominent of these are the ground state and the 2.345-MeV $J^\pi = 5/2^-$ level. The spectrum above these two peaks has
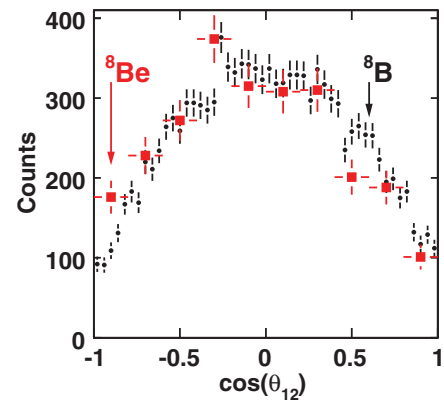

FIG. 18. (Color online) Comparison of angular correlations obtained for the 5.92-MeV state in ^{8}B and the 22.96-MeV state in ^{8}Be. The correlations for the ^{8}Be state were obtained using gates $G10$ and $G11$ in Fig. 17.

been scaled by a factor of 3 to show additional detail. Prominent peaks are also observed at 11.7 and 14.7 MeV. For the latter, two listed levels can contribute, the narrow 14.655-MeV isobaric analog of the ^{9}C ground state and the wider 14.70-MeV ($\Gamma = 1.35$ MeV) state. Judging by the shape of the 14.7-MeV peak, it is likely that both levels are present. As it is impossible to separate the decay modes of these two levels, we will not report on any further analysis of this peak.

The peak at 11.7 MeV is close to a listed 11.640-MeV level with a tentative spin assignment of $J^\pi = 7/2^-$. The width of this listed level (780 ± 45 keV) is also close to the value of 880 ± 80 keV extracted from the peak after correction for the experimental resolution. For further analysis of the correlations associated with this peak, we use the gate $G12$ in Fig. 21(a) with the regions $B5$ and $B6$ on either side to estimate the background under the peak. The ^{8}Be excitation-energy spectra from the α-α pairs associated with each event in the $G12$ gate is plotted in Fig. 21(b). The "background" was not subtracted from this spectrum as the reconstructed ^{8}Be ($\alpha + \alpha$) and ^{9}B ($p + \alpha + \alpha$) excitation energies are highly correlated. This is similar to the strong correlation between the ^{3}He $+ \alpha$ and $p + {}^3$He $+ \alpha$ reconstructed excitation energies found in Sec. IV C1. Due to this correlation, the spectra from gates $B5$ and $B6$ are not good approximations to the background
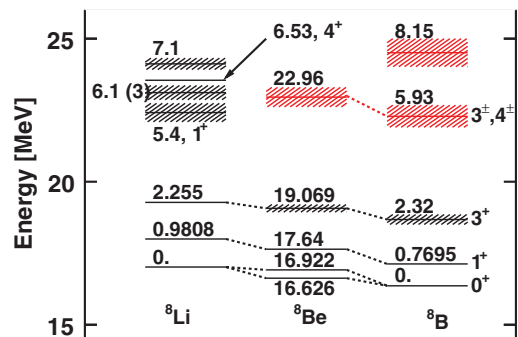

FIG. 19. (Color online) Isobar level diagram of $T = 1$ states for $A = 8$. The levels discussed in this work are displayed in red (gray). The energy scale on the y axis is with respect to the ^{8}Be ground state.
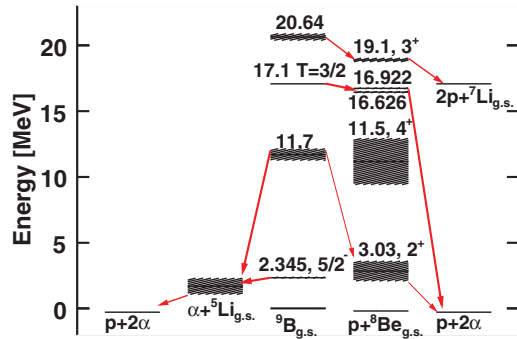
FIG. 20. (Color online) Level diagram for ^{9}B showing the levels discussed in this work and their decay paths. The energy scale on the y axis is with respect to the ^{9}B ground state.

associated with gate $G12$ for the ^{8}Be excitation energy. In Fig. 21(b), contributions from the ^{8}Be ground state and the 3.03-MeV first excited state are clearly present. However, the ground-state contribution is essentially all background because when we gate on this peak and project the ^{9}B excitation-energy distribution, no indication of the 11.7-MeV peak is seen. On the other hand, the 3.03-MeV peak is not all background. With a similar gating arrangement, we find that ~2.8% of the strength at 11.7 MeV is be associated with this ^{8}Be intermediate state.

Most of the 11.7-MeV ^{9}B peak is thus associated with the broad structure above $E^*(^8\text{Be}) = 5$ MeV in Fig. 21(b). This structure overlaps with the wide 11.35-MeV $J^\pi = 4^+$ ^{8}Be level. The situation here is similar to the 8.15-MeV ^{8}B state. The centroid of the structure in Fig. 21(b) is below the centroid for this level, possibly a consequence of sequential feeding. However, the ^{8}Be and ^{9}B excitation energies are well correlated and thus the structure could just be a consequence of this correlation. The alternative intermediate state is ^{5}Li. Figure 21(c) shows the background-subtracted ^{5}Li excitation-energy spectrum associated with the 11.7-MeV peak obtained from the $p + \alpha$ pairs. There are two possible $p + \alpha$ pairs from each $p + 2\alpha$ event and both are included in this spectrum. A peak corresponding to the ground state of ^{5}Li is clearly present indicating that $\alpha + {}^5\text{Li}_{g.s.}$ is an important decay branch.

The correlations associated with the decay of the 11.7-MeV state can be displayed in a manner similar to Fig. 12 where we projected the velocity vectors onto the decay plane. To localize the distribution of α particles, the α-α relative velocity was made parallel to the V_z axis, and as we cannot distinguish the two α particles, we have symmetrized the distributions about $V_z = 0$. The velocity plot for the 11.7-MeV state is displayed in Fig. 22(a) and can be compared to the corresponding plot for the 2.345-MeV state in Fig. 22(c). Unlike Fig. 12 where the protons lie on an arc centered at the origin, the protons in Fig. 22(a) lie on two overlapping arcs each centered approximately near an α particle. These two arcs indicate that the protons are not emitted from the ^{9}B center of mass, as expected for direct proton decay, but come predominantly from the decay of a ^{5}Li intermediate fragment. Thus the broad peak in the α-α excitation spectrum in Fig. 21(b) should not be interpreted as an ^{8}Be excited state.

The distributions in Figs. 22(b) and 22(d) show the results of simulations of a sequential disintegration initiated by an $\alpha +$
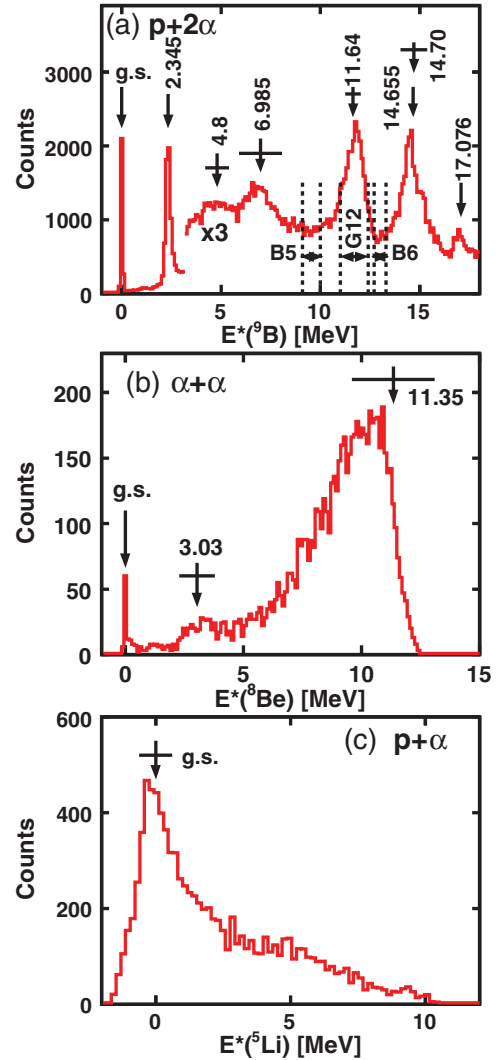

FIG. 21. (Color online) (a) Excitation-energy spectra of ^{9}B derived from $p + 2\alpha$ events. (b) The ^{8}Be excitation-energy spectra obtained from the α-α pairs for events in the 11.7-MeV ^{9}B peak ($G12$ gate). (c) Background subtracted ^{5}Li excitation-energy spectra for events in the 11.7-MeV ^{9}B peak. The arrows indicate the locations of known levels.

^{5}Li$_{g.s.}$ decay. The 2.345-MeV level was previously identified as having strong $\alpha + {}^5\text{Li}_{g.s.}$ decay character [10], however, the two arcs are not separated as the two α particles are located too close together. In both simulations we have determined the emission energies in the two steps using the R-matrix formalism as described in Sec. III. Both simulations reproduce the experimental distribution reasonably well.

Information about the spin of the 11.7-MeV state can be determined from the angular correlations of the two decay steps. Unfortunately as the two arcs overlap, we cannot always identify which α particle is emitted in the first and second steps and thus we cannot uniquely determine θ_{12}. Instead we have looked at the angle $\theta_{2\alpha-p}$ defined in Fig. 23. This is the angle between the relative velocity vectors of the two α particles ($V_{\alpha-\alpha}$) and the proton velocity (V_p) in the ^{9}B center-of-mass frame. Background-subtracted distributions of
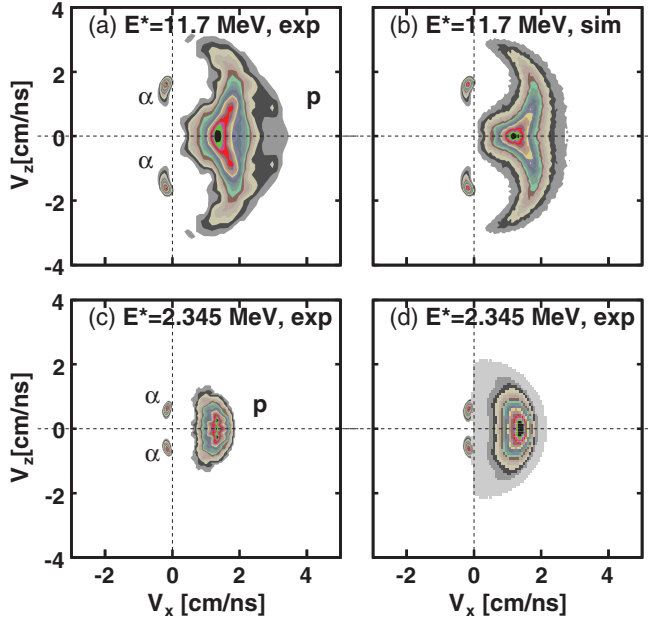
FIG. 22. (Color online) Distributions of the velocities of the three fragments for the $p + 2\alpha$ exit channel associated with (a),(b) the 11.7-MeV and (c),(d) the 2.345-MeV states of ^{9}B. The distributions are projected on the plane of the decay with the two α-particle velocities localized. The experimental distributions in (a),(c) are compared to simulated distributions for α-^{5}Li$_{g.s.}$ decay in (b),(d).
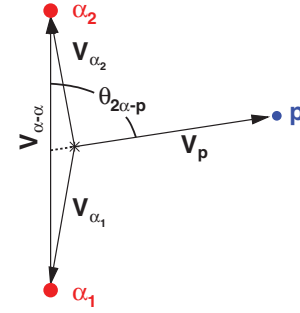

FIG. 23. (Color online) Schematic showing the definition of the angle $\theta_{2\alpha-p}$.

state is clearly resolved in Fig. 25(a) for the 11.7-MeV state.

The discussion of these ^{9}B decays has ignored interactions between the two decay steps. For the 11.7-MeV level, the short lifetime of the ^{5}Li$_{g.s.}$ intermediate state is partially ameliorated by the large kinetic energy released in the first step ($E_k^1 = 10$ MeV). With this value we obtain $R_E = 0.12$ and $d_E = 16$ fm for this decay. The products from the first step thus are separated by ~6 nuclear radii, on average, before the second steps occurs. It is clear that in this case we would expect the
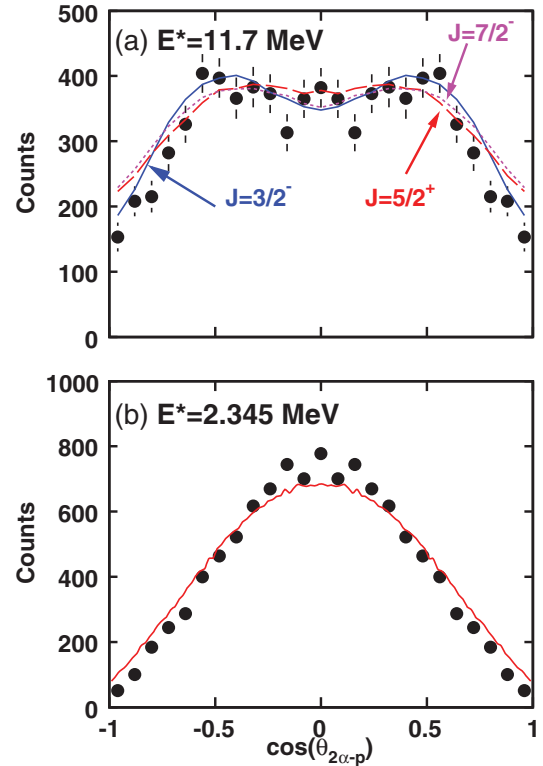
this quantity are shown for both the 11.7- and 2.345-MeV states in Fig. 24. For an initial α-particle decay, unlike proton decay, the angular correlations are sensitive to the parity of the initial level. Furthermore, if we constrain ourselves to α decays with the lowest possible ℓ waves, there is no mixing to consider and each J^π value has a unique correlation. The prediction obtained for the 2.345-MeV level with its known spin of $5/2^-$ is compared to the experimental data in Fig. 24(b). It fits the data extremely well and thus again is consistent with sequential decay initiated by an α-^{5}Li$_{g.s.}$ decay. In Fig. 24(a) for the 11.7-MeV state, we show three predictions which fit the experimental data with $J^\pi = 3/2^-$, $5/2^+$, and $7/2^-$. Of these, the $3/2^-$ predictions give the best fit with a $\chi^2/\nu = 1.7$. The other two cases have $\chi^2/\nu = 2.6$ and 3.0, respectively, so $J^\pi = 3/2^-$ is slightly preferred. We note that the listed 11.64-MeV state in ^{9}B has a tentative assignment as $J^\pi = 7/2^-$, which is the least likely of our three possible fits.

Figure 25 shows the energy correlations for the 11.7- and 2.345-MeV states in ^{9}B. The correlations are presented in the Jacobi Y system where the "core" in Fig. 5 is now the proton and the "protons" in that figure are the α particles. The quantity E_x is now the relative kinetic energy in the p-α subsystem and, for each event, the spectra are incremented twice, once for each of the two p-α pairs. The curves are the R-matrix predictions using parameters for the ^{5}Li$_{g.s.}$ resonance from Ref. [30]. These sequential calculations reproduce the data quite well, further indicating a sequential character to these decays. The strong peak associated with the ^{5}Li ground

FIG. 24. (Color online) Background-subtracted angular correlations measured in the decay of the (a) 11.7-MeV and (b) 2.345-MeV states of ^{9}B. The curves indicate calculated distributions assuming an initial α-^{5}Li$_{g.s.}$ decay. In (a), the calculated results are given for a number of assumed spins for the 11.7-MeV state.
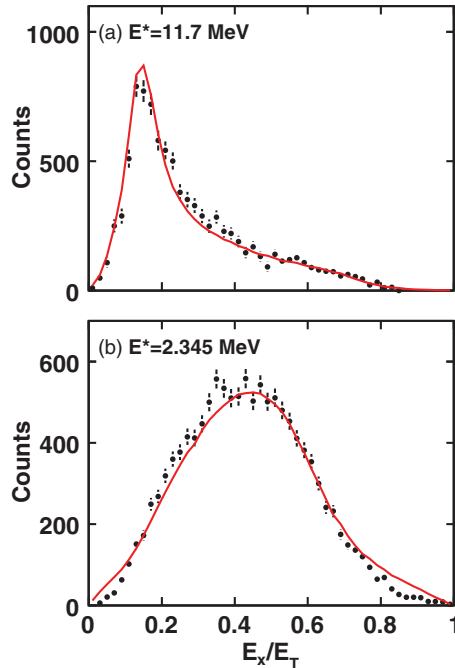
FIG. 25. (Color online) Background-subtracted energy corrections in the Jacobi Y system measured in the decay of the (a) 11.7-MeV and (b) 2.345-MeV states of ^{9}B. The curves indicate calculated distributions assuming α-^{5}Li$_{g.s.}$ decay in the R-matrix approximation.

sequential character of the decay to largely survive final-state interactions between the final fragments.

The sequential character of the 2.345-MeV state is more surprising. Here E_k^1 is much smaller and $R_E = 1.88$ and $d_E = 4.0$ fm and this should be a democratic decay. The value of d_E is in fact one of the smallest values found in this work, even smaller than the value of 6.5 fm obtained for ^{6}Be$_{g.s.}$ decay.

Why does this state have such a strong sequential character, when ^{6}Be$_{g.s.}$ decay displays very little? Specifically we find that the angular correlations associated with sequential decay are found for the 2.345-MeV ^{9}B state, but not for the ^{6}Be$_{g.s.}$ state. A possible reason is that the ^{6}Be$_{g.s.}$ decay is approaching a Goldansky decay; most of the strength of the intermediate state is energetically inaccessible, whereas all the ^{5}Li$_{g.s.}$ strength is accessible for the 2.345-MeV state. Another consideration is that final-state interactions between the products would be largest for $\cos(\theta_{2\alpha-p}) = \pm 1$, i.e., when one of the fragments from the second step is directed directly toward the α particle from the first step. However, the angular corrections are minimal for these cases and so the effect of final-state interactions will also be minimized. Although the correlations do maintain a strong sequential character, the magnitude of the decay width cannot be explained from a R-matrix calculation (Sec. III). The R-matrix prediction by Barker was a factor of 4 too small [31], indicating the need for a three-body calculation.

One can also look for ^{9}B levels which decay predominantly to ^{8}Be states. The reconstructed ^{8}Be excitation-energy spectrum from the α-α pairs of each $p + 2\alpha$ event is shown in Fig. 26(a). The ^{8}Be ground state and a number of excited
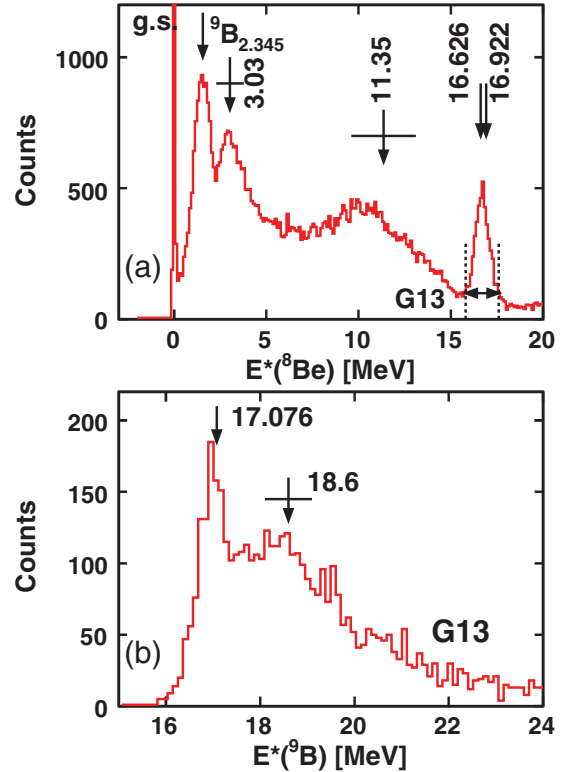

FIG. 26. (Color online) (a) Excitation-energy distribution for ^{8}Be fragments reconstructed from the α-α pairs of all $p + 2\alpha$ events. (b) The ^{9}B excitation-energy distributions obtained with the $G13$ gate on the ^{8}Be excitation energy.

states indicated by the arrows are clearly present. The peak at $\sim$1.5 MeV is not a ^{8}Be excited state, but rather is associated with the decay of the 2.345-MeV ^{9}B excited state. Of particular interest is the strong peak associated with the 16.626- and 16.922-MeV mixed $T = 0 + 1$ $J^\pi = 2^+$ states. These are narrow states, but the experimental resolution is not sufficient for their separation. The peak thus can contain contributions from both of these mixed-isospin states.

The ^{9}B excitation-energy spectrum obtained by gating of the $E^* \sim 17$-MeV peak [gate $G13$ in Fig. 26(a)] is shown in Fig. 26(b). The peak at 16.99 ± 0.04 MeV is clearly isolated although it was also present in the ungated spectrum of Fig. 21(a). This peak could correspond to a previously known level at 16.71 ± 0.10 MeV or the 17.076 ± 0.04-MeV $T = 3/2$ level. Both decays satisfy isospin conservation and the former, if it has a significant $d + ^7$Be branching ratio, may be important in big-bang nucleosynthesis [32]. The magnitude of the yield in the observed peak is consistent with that from the ungated spectrum in Fig. 21(a) indicating that this state predominantly decays to one or both of the ^{8}Be $T = 0 + 1$ levels. Presumably most of the decay is to the 16.626-MeV state as only the low-energy tail of the 16.922-MeV state is energetically accessible.

The 16.71-MeV level has only been observed before in one experimental study [33], where it was suggested to be the mirror of the 16.67-MeV $J^\pi = 5/2^+$ state in ^{9}Be. Experimental angular distributions in that work were consistent with this spin assignment. The spin of the 17.076-MeV state
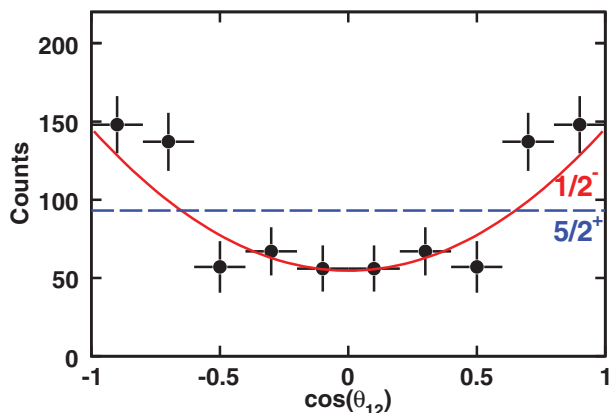
FIG. 27. (Color online) Angular correlation for the 16.99-MeV state in ^{9}B. Data points indicate the background-subtracted experimental results and the curves shows the results expected for the indicated level spins.

is not listed in the ENSDF database, however, it is probably the mirror of the 16.977-MeV $T = 3/2$ ^{9}Be state, which has a spin of $J^\pi = 1/2^-$. In the two cases we would thus expect the first step in the sequential decay would be dominated by $\ell = 0$ and 1 decay, respectively, giving rise to different angular correlations.

We have extracted the angular correlation between the first proton emission step and the second 2α decay step for the events in the peak located at $\sim$17 MeV in Fig. 26(b). The higher-energy region directly adjacent in excitation energy was used for the background subtraction. The background-subtracted correlation is plotted in Fig. 27 and is compared to calculations for $J^\pi = 1/2^-$ ($\ell = 1$) and $J^\pi = 5/2^+$ ($\ell = 0$). Of these calculations, the data are in much better agreement with the $J^\pi = 1/2^-$ case, suggesting that the state observed is the $T = 3/2$ state. The decay to the 16.626-MeV state is $R_E = 0.41$ and $d_E = 45$ fm, and the large value of the latter number suggests this is approaching a truly sequential decay.

2. $2p + {}^7Li$ exit channel

Due to the problem with the saturation of the amplifiers, only a small fraction of the ^{7}Li fragments could be identified. However, there were sufficient statistics for the $2p + {}^7$Li exit channel to isolate a new level in ^{9}B. The excitation-energy spectrum determined from $2p + {}^7$Li events is displayed in Fig. 28(a) and a peak at 20.64 ± 0.10 MeV is evident with a width of $\Gamma = 450 \pm 250$ keV. The large error is a consequence of an uncertainty of how to define the background when fitting this peak. We do not know whether the ^{7}Li fragment was created in the ground state or the γ-emitting 0.477-MeV excited state. The energy of the level could thus be either 20.64 or 21.12 MeV. We have attempted to see if the decay of this level could be associated with a sequential two-proton decay through a ^{8}Be excited state. As there are two protons, we can reconstruct the two possible ^{8}Be excitation energies from each $2p + {}^7$Li event. The background-subtracted distribution of both of these gated on the 20.64-MeV peak [gate G14 in Fig. 28(a) with background gates $B7$ and $B8$] is shown in
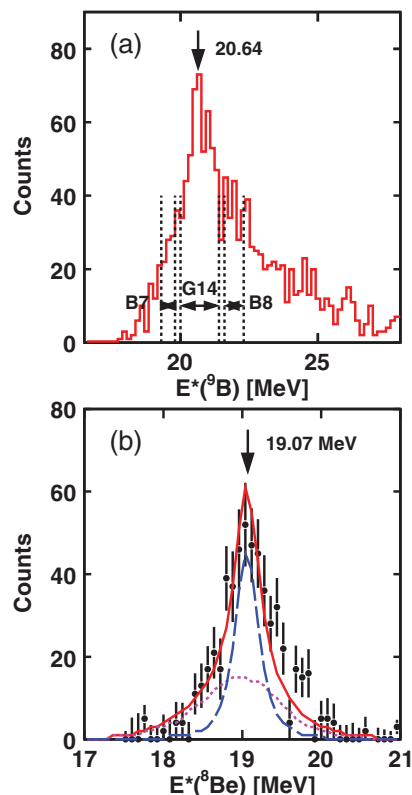

FIG. 28. (Color online) (a) Excitation-energy distribution for ^{9}B fragments reconstructed from $2p + {}^7$Li events. (b) The ^{8}Be excitation-energy distributions obtained with the $G14$ gate on the ^{9}Be excitation energy. The distributions contains contributions from both possible p-^{7}Li combinations.

Fig. 28(b). Again there is some uncertainty in the background subtraction, but the location of the peak was not affected by this. The peak can be identified with the 19.069-MeV, $\Gamma = 271$ keV, $J^\pi = 3^+$ in ^{8}Be. The curves in Fig. 28(b) show Monte Carlo simulations of the decay through this state. The long- and short-dashed curves show the contributions from the correctly and incorrectly identified proton associated with ^{8}Be decay, and the solid curve is the sum of these two. Both the correct and incorrect distributions have almost the same average energy, but the incorrect distribution is quite wide and the peak position is defined by the correctly identified proton, which has a much narrower distribution. The simulation was performed assuming the second decay is to the ground state of ^{7}Li. If we assumed the decay was to the 0.477-MeV state, then the reconstructed ^{8}Be peak energy would be at $\sim$19.5 MeV. No previously known ^{8}Be excited state could be found at this energy but it is possible that decays occur through an unknown ^{8}Be excited state, however it seems more likely that the decay is to the ^{7}Li ground state through the known 19.07-MeV state.

F. ^{10}C levels

Information on ^{10}C states produced by neutron pickup and more complicated reactions was obtained from the $2p + 2\alpha$ exit channel. This is the only channel available for
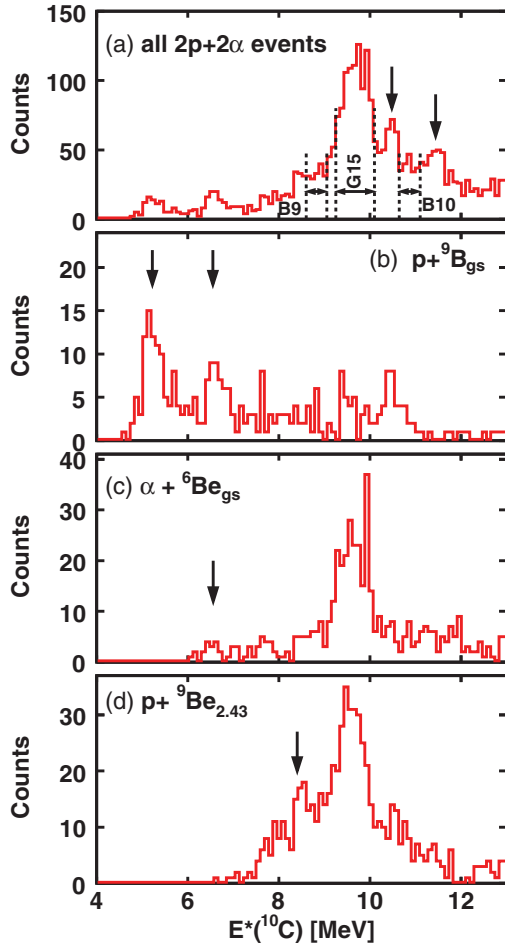
FIG. 29. (Color online) Excitation-energy distributions for ^{10}C fragments reconstructed from $2p + 2\alpha$ events. Panel (a) is for all events, while (b)–(d) are gated on the presence of $^9B_{g.s.}$, $^6Be_{g.s.}$, and $^9B_{2.345}$ intermediate states. Arrows show the locations of the peaks discussed in this work. The gate $G15$ used to select the 9.69-MeV peak and the gates $B9$ and $B10$ used for background subtraction are indicted.

particle-decaying states with $E^* < 15$ MeV. The excitation-energy spectrum from all of these events is displayed in Fig. 29(a) and is dominated by a peak at 9.69 MeV, although other smaller peaks are evident. In our previous work, levels for this exit channel were revealed by gating on the presence of various narrow intermediate states [23]. Figures 29(b)–29(d) show the ^{10}C excitation-energy distribution gated on the ^9B ground state, the ^6Be ground state, and the 2.345-MeV ^9B excited state, respectively.

The arrows in Fig. 29(b) show the locations of two states (5.222 and 6.553 MeV) that were excited via the inelastic scattering of a ^{10}C beam and which decay by proton emission to the ^9B ground state [23]. These states dominated the total ^{10}C excitation-energy spectrum in inelastic scattering, but here they are weakly populated and require a gate by the $^9B_{g.s.}$ to enhance them [see Fig. 29(b)]. As these states are expected to have 2α cluster structure [23], it is not surprising that a neutron pickup by ^9C (which does not have any 2α cluster structure) does not populate these states strongly.

The widths of these states also appear to be wider (by 50–70%) than we would expect based on the intrinsic widths given in Ref. [23] and the simulated experimental resolution. Possibly these peaks are actually doublets, which would not be surprising as other levels near these energies are expected based on the mirror nucleus ^9Be. At higher excitation energies in Fig. 29(b), there may also be indications of other states, though the statistical errors are large. We note the absence of any significant contribution from the 9.69-MeV level in this spectrum.

A 6.56-MeV state which decayed via the $\alpha + {}^6Be_{g.s.}$ channel was also observed in the inelastic excitation of a ^{10}C beam [23,34]. Its location is indicated by the arrow in Fig. 29(c). This state is also expected to have strong cluster structure and is clearly only weakly populated in the present experiment. In Fig. 29(c), the spectrum is again dominated by the 9.69-MeV peak, indicating that $\alpha + {}^6Be_{g.s.}$ is an important decay branch for this level.

The spectrum in Fig. 29(d) is also dominated by the 9.69-MeV level indicating that this level has a second decay branch ($p + {}^9B_{2.345}$). Also a smaller peak appears at 8.5 MeV. The arrow in this figure shows the location of an 8.4-MeV state that was previously shown to decay through the 2.345-MeV ^9B intermediate level. However, the intrinsic width of that state was ~1 MeV, significantly wider than the present peak. The experimental width of the peak in this work (~300 keV) is consistent with the simulated resolution. Within the statistical uncertainties we estimate $\Gamma < 200$ keV.

Other small peaks are also suggested in the total distribution in Fig. 29(a). The peaks at 10.48 and 11.44 MeV, indicated by the arrows in this figure, are previously unknown. Their widths are consistent with the experimental resolution. The decay of these states is not known; they do not feature prominently in the distributions gated by the long-lived intermediates.

1. 9.69-MeV state

The strong 9.69-MeV state is wider than the other observed ^{10}C states; from the simulation we estimate that its intrinsic width is 490 keV. It was not observed via ^{10}C inelastic scattering in Refs. [23,34], suggesting that it does not have a strong cluster structure and maybe is more single particle in nature. In any case we will show that its decay modes are quite interesting. In the following we give an analysis of correlations associated with this peak using gate $G15$ and background gates $B9$ and $B10$ in Fig. 29(a). All the distributions discussed in the remainder of this section are background subtracted.

As we have observed in Figs. 29(c) and 29(d) that the 9.69-MeV level has strength for decays into the $\alpha + {}^6Be_{g.s.}$ and $p + {}^9B_{2.345}$ channels. Estimates of the branching ratios for these two channels are based on the ^6Be and ^9B excitation-energy spectra gated on the 9.69-MeV state displayed in Fig. 30. One can clearly see peaks associated with ^6Be ground state [Fig. 30(b)] and the 2.345-MeV state [Fig. 30(a)] in ^9B. The yield associated with the ground state of ^9B is clearly minimal. The yield in the ^6Be and $^9B_{2.345}$ peaks were fit with Gaussians with smooth backgrounds. From these yields, and correcting for the detector efficiency, we determine branching
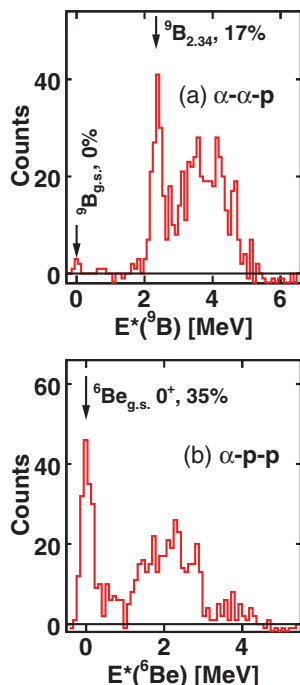
FIG. 30. (Color online) Background-subtracted excitation-energy distributions for (a) ^{9}B and (b) ^{6}Be fragments produced in the decay of the 9.69-MeV level of ^{10}C determined from $p + 2\alpha$ and $2p + \alpha$ triplets.
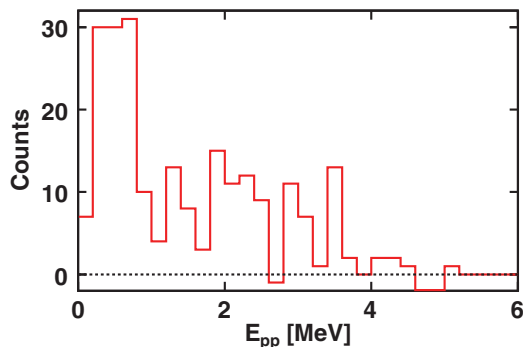

FIG. 31. (Color online) Distribution of relative kinetic energy between the two protons for the 9.69-MeV level in ^{10}C.

pairs are consistent with the ^{5}Li$_{g.s.}$ resonance. The decay thus appears to be four body in nature and cannot be described by a sequential process. A possible interpretation is that all four p-α pairs are simultaneously in ^{5}Li$_{g.s.}$ resonances and some fraction of the p-p pairs are tightly correlated in a "diproton." Possibly, the α-α pair may also be in a 3.03-MeV ^{8}Be resonance. On the other hand, the overlap

ratios of 35% and 17% for $\alpha + {}^6$Be$_{g.s.}$ and $p + {}^9$B$_{2.345}$ decay paths, respectively. Both of these decay branches are safely sequential with $d_E = 136$ and 200 fm, respectively. The determination of the decay mechanism of the remaining $\sim$50% of the yield is more difficult and, to isolate this component, we have vetoed events associated with the ^{6}Be$_{g.s.}$ and ^{9}B$_{2.435}$ peaks in the following analysis.

The distribution of E_{pp}, the relative kinetic energy between the two protons, is plotted in Fig. 31. This distribution shows a strong enhancement at small relative energies ($E_{pp} < 1.0$ MeV), the diproton region, but also displays a tail to significantly higher values. Figures 32(a) and 32(b) show the distributions of ^{8}Be and ^{5}Li excitation energy determined from the detected α-α pairs and all four combinations of p-α pairs. The total distributions (circular data points) have strong overlaps with the wide 3.03-MeV ^{8}Be and the ^{5}Li ground-state resonances, respectively. The distributions are rather insensitive to whether the events are associated with the diproton peak in Fig. 31 or associated with the higher-energy tail. To illustrate this, the squared data points in Figs. 32(a) and 32(b) show the distributions gated on the diproton peak ($E_{pp} < 1.0$ MeV). Within the statistical uncertainties, they are the same shape as the ungated distributions.

The strong overlap with the ^{5}Li$_{g.s.}$ resonance may initially suggest that the ^{10}C fragment decays via the ^{5}Li$_{g.s.} + {}^5$Li$_{g.s.}$ channel. However, in such a case, the excitation energy reconstructed from an α particle and a proton originating from different ^{5}Li fragments should populate the ^{5}Li excitation energies significantly higher than the ^{5}Li$_{g.s.}$ resonance region. However, the experimental data indicated that all four α-p
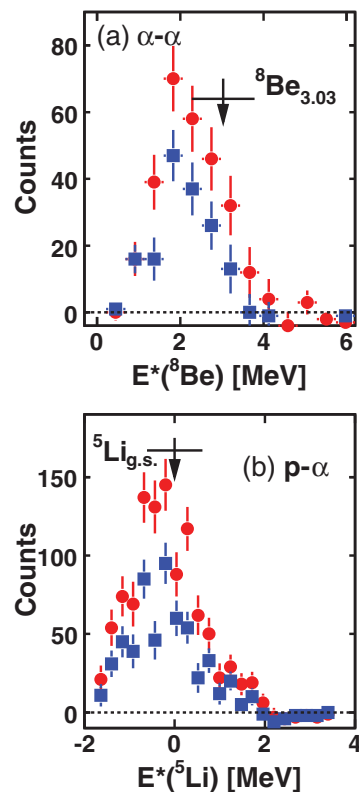

FIG. 32. (Color online) Background-subtracted excitation-energy distributions for (a) ^{8}Be and (b) ^{5}Li fragments produced in the decay of the 9.69-MeV level of ^{10}C determined from α-α and p-α pairs. For the latter case, the distribution contains all four possible p-α pairs associated with each detected $2p + 2\alpha$ event. The distributions indicated by the circular data points have no restriction on the p-p relative energy, while for the squared-shaped data points $E_{pp} < 1.0$ MeV. The arrows with error bars show the mean energy and width of the indicated resonances.
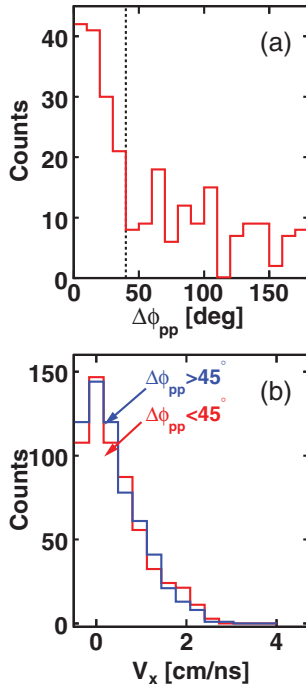
FIG. 33. (Color online) Background-subtracted distributions associated with the decay of the 9.69-MeV state in ^{10}C. (a) Distribution of the angle $\Delta\phi_{pp}$. This is the angle between the two planes in velocity space defined by the two α particles and each of the protons. (b) For the two indicated gates on $\Delta\phi_{pp}$, the distributions of the x component of the proton velocity (see text). For comparison purposes, the results for $\Delta\phi_{pp} > 40°$ have been normalized to the same number of counts as in the $\Delta\phi_{pp} < 40°$ distribution.

with the ^{5}Li$_{g.s.}$ and other resonances may just be coincidental. If all of these associations with resonances are correct, it is not clear that a configuration exists which would satisfy all of the implied angular momentum couplings. To display the correlations graphically, we note that each $p + 2\alpha$ triplet in each $2p + 2\alpha$ event defines a plane in velocity space. With the two protons, we define two such planes in each event. The distribution of $\Delta\phi_{pp}$, the angle between these two planes, is plotted in Fig. 33(a). This distribution resembles the relative-proton-energy distribution in Fig. 31 with a diproton region and a high-energy tail, and in fact the quantities E_{pp} and $\Delta\phi_{pp}$ are strongly correlated.

In order to help visualize the correlations between each proton and the two α particles, we have employed the procedure used to generate Fig. 12. For each $p + 2\alpha$ triplet, the α-particle and proton velocity vectors are projected into their decay plane. Subsequently they are rotated in this plane to align the locations of the α particles. The two-dimensional velocity distributions are plotted in Fig. 34 for gates on the diproton region ($\Delta\phi_{pp} < 40°$) and the high-energy tail ($\Delta\phi_{pp} > 40°$).

Both distributions are quite similar and thus again there is little difference in the p-α correlations for the diproton and high-energy tail regions of the p-p relative energy. This is further illustrated in Fig. 33(b) where the projected V_x distributions for these two regions are compared. Again we see very little difference in the results for the two gates. The average location of the two α particles and the proton
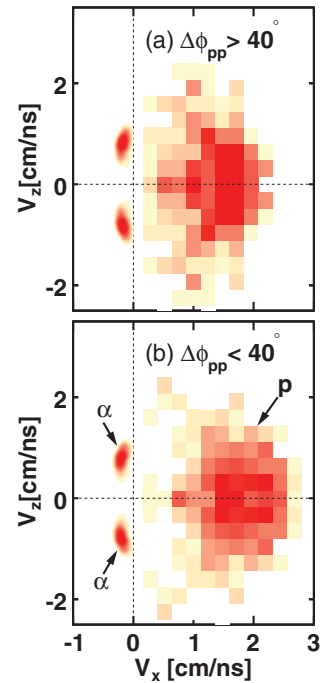

FIG. 34. (Color online) Velocity distributions of α particles and protons produced in the decay of the 9.69-MeV state in ^{10}C. For each $2\alpha + p$ triplet in each detected $2\alpha + 2p$ event, the velocities have been projected onto the plane of the three fragments and rotated in this plane to align the locations of the α particles. The results are shown for (a) $\Delta\phi_{pp} < 40°$ and (b) $\Delta\phi_{pp} > 40°$ where the $\Delta\phi_{pp}$ is the angle between the two planes defined by the two protons.

form an isosceles triangle in their defining plane; i.e., the two p-α average relative velocities are identical and thus all p-α pairs can have the same reconstructed ^{5}Li excitation energy. Four-body decay of ^{10}C excited states with $E^* \sim 9$ MeV was also suggested in Ref. [35].

V. DISCUSSION AND CONCLUSIONS

This work highlights the wide range of many-particle decays of ground and excited states in light nuclei. It is not clear that there is a simple way of predicting when the decays should be sequential or prompt. Certainly the presence of possible narrow intermediate states does not guarantee that the system will take advantage of them. For example, the 9.69-MeV state in ^{10}C has ^{6}Be$_{g.s.}$ and ^{9}B$_{2.34}$ intermediate states with $\Gamma \sim$ 90 keV; yet 50% of the time it bypasses these and undergoes a four-body decay. The 6.56-MeV state ^{10}C also has competing prompt and sequential decay branches [23]. The nature of the decay is certainly related to the structure of the state and, in principle with suitable models, this information can be used to improve structure calculations. Presently there are only a few cases where prompt three-body decay has been modeled in a sophisticated manner, as, for example, the quantum-mechanical cluster calculation [6], where comparisons to experimental correlations are useful. The prompt four-body decay poses an even more difficult theoretical problem.

In this work we have studied many-particle exit channels associated with states formed following the interactions of

an $E/A = 70$ MeV ^{9}C beam with a ^{9}Be target. The decay products were detected in the HiRA array and the states were identified from the invariant mass of the detected fragments. Correlations between these fragments were used to deduce the nature of the decay and search for long-lived intermediate states associated with sequential decay processes. For such decays, angular correlations between the fragments provide information on the spin of the level.

The ground state of ^{8}C disintegrates into four protons and an α particle. This decay was found to proceed through the ^{6}Be$_{g.s.}$ intermediate state, with two steps of two-proton decay. The correlations between the protons in the first step exhibit a significant enhancement in a region of phase space where the two protons have small relative energy. The correlations in the second step were found to be consistent with ^{6}Be$_{g.s.}$ two-proton decay obtained from an independent measurement using a ^{7}Be beam.

Evidence suggests that the isobaric analog of this state in ^{8}B, undergoes two-proton decay to the isobaric analog of ^{6}Be$_{g.s.}$ in ^{6}Li. This is the first case of two-proton decay between two isobaric analog states. The exact nature of the two-proton decay awaits future measurements, but it may constitute a Goldansky-type decay with a single proton emission being energetically allowed but isospin forbidden.

A 9.69-MeV state of ^{10}C was found, which $\sim$50% of the time undergoes a prompt four-body decay into the $2p + 2\alpha$ channel. There is a strong diprotonlike correlation between the two protons; at the same time, all four possible p-α pairs have energies consistent with a ^{5}Li$_{g.s.}$ resonance. No sequential decay scenario is possible to produce four simultaneous ^{5}Li$_{g.s.}$ resonances.

Evidence for a prompt three-body decay of the 8.15-MeV state of ^{8}B was found. On the other hand, a number of states with three-body exit channels were observed that are well described as sequential decays through intermediate states. These include the isobaric pair, ^{8}B$_{5.93}$ and ^{8}Be$_{22.9}$, and the 11.7-, 16.9-, and 20.6-MeV states of ^{9}B. The correlations in the decay of the 2.345-MeV state of ^{9}B to the $p + 2\alpha$ channel were found to have strong sequential character associated with a ^{5}Li intermediate, even though the lifetime of this intermediate state is very short and, at the very least, we would expect there to be very important final-state interactions.

Finally, new mass excesses and decay widths were obtained for the ground states of ^{7}B and ^{8}C.

ACKNOWLEDGMENTS

[1] V. I. Goldansky, Nucl. Phys. **19**, 482 (1960).

[2] K. Miernik *et al.*, Phys. Rev. Lett. **99**, 192501 (2007).

[3] B. Blank *et al.*, Phys. Rev. Lett. **94**, 232501 (2005).

[4] O. V. Bochkarev, L.. V. Chulkov, A. A. Korsheninnikov, E. A. Kuz'min, I. G. Mukha, and G. B. Yankov, Nucl. Phys. A **505**, 215 (1989).

[5] D. F. Geesaman, R. L. McGrath, P. M. S. Lesser, P. P. Urone, and B. VerWest, Phys. Rev. C **15**, 1835 (1977).

[6] L. V. Grigorenko *et al.*, Phys. Rev. C **80**, 034602 (2009).

[7] R. J. Charity *et al.*, Phys. Rev. C **82**, 041304 (2010).

[8] M. S. Wallace *et al.*, Nucl. Instrum. Methods Phys. Res. A **583**, 302 (2007).

[9] G. L. Engel, M. Sadasivam, M. Nethi, J. M. Elson, L. G. Sobotka, and R. J. Charity, Nucl. Instrum. Methods Phys. Res. A **573**, 418 (2007).

[10] R. J. Charity *et al.*, Phys. Rev. C **76**, 064313 (2007).

[11] J. F. Ziegler, J. P. Biersack, and U. Littmark, *The Stopping and Range of Ions in Solids* (Pergamon, New York, 1985); the code SRIM can be found at [http://www.srim.org].

[12] R. Anne, J. Herault, R. Bimbot, H. Gauvin, C. Bastin, and F. Hubert, Nucl. Instrum. Methods Phys. Res. B **34**, 295 (1988).

[13] R. J. Charity *et al.*, Phys. Rev. C **78**, 054307 (2008).

[14] A. M. Lane and R. G. Thomas, Rev. Mod. Phys. **30**, 257 (1958).

[15] F. C. Barker, Phys. Rev. C **59**, 535 (1999).

[16] L. C. Biedenharn and M. E. Rose, Rev. Mod. Phys. **25**, 729 (1953).

[17] H. Frauenfelder, Annu. Rev. Nucl. Sci. **2**, 129 (1953).

[18] Evaluated Nuclear Structure Data File (ENSDF), [http://www.nndc.bnl.gov/ensdf/].

[19] G. Audi, A. H. Wapstra, and C. Thibault, Nucl. Phys. A **729**, 337 (2003).

[20] R. G. H. Robertson, S. Martin, W. R. Falk, D. Ingham, and A. Djaloeis, Phys. Rev. Lett. **32**, 1207 (1974).

[21] R. G. H. Robertson, W. Benenson, E. Kashy, and D. Mueller, Phys. Rev. C **13**, 1018 (1976).

[22] R. E. Tribble, R. A. Kenefick, and R. L. Spross, Phys. Rev. C **13**, 50 (1976).

[23] R. J. Charity, T. D. Wiser, K. Mercurio, R. Shane, L. G. Sobotka, A. H. Wuosmaa, A. Banu, L. Trache, and R. E. Tribble, Phys. Rev. C **80**, 024306 (2009).

[24] S. Cohen and D. Kurath, Nucl. Phys. **73**, 1 (1965); **101**, 1 (1967).

[25] F. C. Barker, Phys. Rev. C **66**, 047603 (2002); **67**, 049902(E) (2003).

[26] B. A. Brown and F. C. Barker, Phys. Rev. C **67**, 041304 (2003).

[27] R. L. McGrath, J. Cerny, and E. Norbeck, Phys. Rev. Lett. **19**, 1442 (1967).

[28] L. Grigorenko, R. Johnson, I. Mukha, I. Thompson, and M. Zhukov, Eur. Phys. J. A **15**, 125 (2002).

[29] R. G. H. Robertson, W. S. Chien, and D. R. Goosman, Phys. Rev. Lett. **34**, 33 (1975).

[30] C. L. Woods, F. C. Barker, W. N. Catford, L. K. Fifield, and N. A. Orr, Aust. J. Phys. **41**, 525 (1988).

[31] F. C. Barker, Phys. Rev. C **68**, 054602 (2003).

[32] N. Chakraborty, B. D. Fields, and K. A. Olive, Phys. Rev. D **83**, 063006 (2011).

[33] S. Dixit *et al.*, Phys. Rev. C **43**, 1758 (1991).

[34] N. Curtis *et al.*, Phys. Rev. C **77**, 021301 (2008); **82**, 029907(E) (2010).

[35] F. Grenier *et al.*, Nucl. Phys. A **811**, 233 (2008).